

# Testing Chameleon Theories with Light Propagating through a Magnetic Field

Philippe Brax,<sup>1</sup> Carsten van de Bruck,<sup>2</sup> Anne-Christine Davis,<sup>3</sup> David F. Mota,<sup>4</sup> and Douglas Shaw<sup>5</sup>

<sup>1</sup> *Service de Physique Théorique CEA/DSM/SPHT,  
Unité de recherche associée au CNRS, CEA-Saclay F-91191 Gif/Yvette cedex, France.*

<sup>2</sup> *Department of Applied Mathematics, The University of Sheffield,  
Hounsfield Road, Sheffield S3 7RH, United Kingdom*

<sup>3</sup> *Department of Applied Mathematics and Theoretical Physics,  
Centre for Mathematical Sciences, Cambridge CB2 0WA, United Kingdom*

<sup>4</sup> *Institut für Theoretische Physik, Universität Heidelberg,  
Philosophenweg 16/19, D-69120 Heidelberg, Germany*

<sup>5</sup> *Centre for Mathematical Sciences, Cambridge CB2 0WA, United Kingdom*

It was recently argued that the observed PVLAS anomaly can be explained by chameleon field theories in which large deviations from Newton's law can be avoided. Here we present the predictions for the dichroism and the birefringence induced in the vacuum by a magnetic field in these models. We show that chameleon particles behave very differently from standard axion-like particles (ALPs). We find that, unlike ALPs, the chameleon particles are confined within the experimental set-up. As a consequence, the birefringence is always bigger than the dichroism in PVLAS-type experiments.

PACS numbers: 14.80.-j, 12.20.Fv

## I. INTRODUCTION

Light scalar fields are common in theories of physics beyond the standard model. These scalar fields can couple to both the standard model fields as well as to new types of matter. Since experiments have not yet detected new forces, it means that the force mediated by these scalar fields is either very weak (with a strength less than gravity) or short-ranged in the laboratory. In string theory, for example, there are many moduli fields which couple to matter with gravitational strength. The chameleon mechanism provides a way to suppress the forces mediated by these scalar fields via non-linear field self-interactions and interactions with the ambient matter [1, 2]. As a result, the masses of the scalar fields become dependent on the ambient matter density; this is the reason why these fields have been dubbed chameleon fields. If the observed accelerated expansion of the universe is due to a chameleon-like field, it has interesting cosmological consequences [3, 4].

An obvious way to look for chameleon fields are gravitational experiments in different environments [1, 2]. Additionally, it was recently pointed out that chameleon fields are a natural way to reconcile the PVLAS and CAST results [5]. In 2006, it was reported that the PVLAS experiment had detected light polarization rotation in the vacuum in the presence of a magnetic field, [6]. Recently there has been a lot of activity concerning the theoretical interpretation of this detection, see e.g. [7]–[22] for recent work. In particular, this finding could be seen as evidence for the presence of an axion-like particle (ALP) or milli-charged particles. The PVLAS 2006 results can be explained if the mass of the ALP is of order  $m_{\text{ALP}} \approx 10^{-3}$  eV and the inverse coupling constant to two photons is  $M \approx 10^5$  GeV. These results are in direct conflict with the CAST results, because, for these parameters, axions emitted in the sun should have been detected by this experiment. However, as was pointed out in [5], assuming the values for  $m$  and  $M$  given above, both results can be explained if the particle behaves like a chameleon field, because the mass of the field inside the PVLAS experiment would then be very different from the mass of the field inside the Sun. In the Sun, the chameleon mass is so high that chameleon particles cannot be photo-produced. Additionally, it was shown in [5] that the new force mediated by the chameleon field is not in conflict with current experiments.

Although in a context different from chameleon theories, the potential resolution of conflict between the CAST and the PVLAS experiments provided by particles with an environmentally dependent mass was also discussed in Ref. [8]. It was also pointed out that if the particle mass outside the cavity was much larger than inside, then ALPs would be reflected in the same way as the photons and *not* escape from the Fabry-Perot cavity. As an implication, there would be no signal found in "light shining through the wall" experiments [8]. As the BMV collaboration seems to have observed [9]. It should be noted that in Ref. [8] the ALPs were assumed to reflect in exactly the same way as the photons; we see below that this is not the case if the ALP is a chameleon. The predictions of the chameleon model are therefore very different from the ones of reflecting ALP model consider in Ref. [8].

Recently new PVLAS results have been reported [10]. These new results do *not* confirm the previously reported rotation. Indeed they find no evidence for either rotation or ellipticity with a 2.3 T magnetic field. The initial PVLAS results were found using a 5.5 T magnetic field. With a 5.5 T field, the new results additionally show no evidence for any rotation, however a non-zero ellipticity is still detected. In the context of standard ALPs (but not necessarily chameleon fields), however, the detected ellipticity is excluded with a 99% confidence by the null result found with

the 2.3 T magnetic field. Although it might be an artefact, the ellipticity for  $B = 5.5$  T can be explained with a chameleon model with  $m \approx 10^{-3}$  eV and  $M \approx 10^6$  GeV. Future experiments will give us decisive clues later this year.

In this paper we study the behaviour of chameleon particles inside optical experiments similar to PVLAS. The aim of this paper is to derive the expression for the rotation and the ellipticity of the laser light. As we will show, chameleon particles and standard ALPs behave very differently. Firstly, because the mass of the particles depend on the environment and they do not have enough energy, chameleon particles cannot leave the experimental region. In contrast to ALPs, which do leave the interaction region, chameleon particles are therefore trapped inside the experimental set-up. Secondly, because the mass of the particles varies inside the experiment, chameleon particles and photons reflect differently. As we will discuss, this results in a very different form for the expressions for the predicted rotation and ellipticity.

The paper is organized as follows: In Section II we present the chameleon model in more detail. In Section III we discuss how the chameleon mass behaves inside the experimental set-up. The behaviour of chameleon particles in experiments like PVLAS is described in Section IV. The predictions made by the chameleon model are discussed in Section V. We conclude in Section VI. Mathematical details can be found in the Appendices.

## II. THE CHAMELEON MODEL

Chameleon theories are essentially scalar field theories with a self-interaction potential and couplings to matter; they are specified by the action

$$S = \int d^4x \sqrt{-g} \left( \frac{1}{2\kappa_4^2} R - g^{\mu\nu} \partial_\mu \phi \partial_\nu \phi - V(\phi) - \frac{e^{\phi/M}}{4} F^2 \right) + \sum S_m^{(i)}(e^{\phi/M_i} g_{\mu\nu}, \psi_m^{(i)}) \quad (1)$$

where the  $S_m^{(i)}$  and  $\psi_m^{(i)}$  are respectively the matter actions and matter fields. The couplings to matter and the electromagnetic sector are specified by the mass scales  $M_i$  and  $M$  respectively. For simplicity we take the coupling of the scalar field to matter and to the electromagnetism to be universal (i.e.  $M_i = M$ ). In more general theories one would not expect a truly universal coupling. Our conclusions are, however, not affected by this assumption. The coupling to matter implies that particle masses in the Einstein frame depend on the value of  $\phi$

$$m(\phi) = e^{\phi/M} m_0 \quad (2)$$

where  $m_0$  is the bare mass as appearing in  $S_m$ . The strength of the chameleon to matter coupling is given by

$$\beta = \frac{M_{Pl}}{M}. \quad (3)$$

where  $M_{Pl} = 1/\sqrt{8\pi G} \approx 2.4 \times 10^{18}$  GeV. As we show in Section IV, if a theory such as this is to be detected by axion searches one must require that  $M \ll M_{Pl}$ . This implies that on scales smaller than  $\hbar c/m_\phi$ , where  $m_\phi$  is the mass of  $\phi$ , the chameleon force between matter particles is  $2(M_{Pl}/M)^2 \gg 1$  times stronger than their mutual gravitational attraction. If the mass,  $m_\phi$ , of  $\phi$  is a constant then one would then have to require that  $m_\phi \gg 1$  meV otherwise such a theory would already be ruled out by experimental tests of Newton's law. Another, and potentially far more interesting prospect, is that the mass of the scalar field grows with the background density of matter. In high density regions it could then be large enough to satisfy the constraints coming from tests of gravity, whilst being small enough to produce detectable alterations to the standard physical laws in low density regions. Scalar fields that have this property are said to be Chameleon fields. In addition to the couplings to matter, chameleon fields have non-linear self-interactions described by a potential  $V(\phi)$ . Assuming an exponential coupling to matter of the form given by Eq. (1), a scalar field theory will have a chameleon mechanism, for some range of  $\phi$ , provided that:

$$V'(\phi) < 0, \quad V'' > 0, \quad V'''(\phi) < 0, \quad (4)$$

where  $V' = dV/d\phi$ . Whether or not the chameleon mechanism is strong enough to evade current experimental constraints depends partially on the details of the theory, i.e.  $V(\phi)$  and  $M$ , and partially on the initial conditions [3]. For exponential couplings and a potential of the form

$$V(\phi) = \Lambda^4 \exp(\Lambda^n/\phi^n) \approx \Lambda^4 + \frac{\Lambda^{4+n}}{\phi^n} \quad (5)$$

the chameleon mechanism can in principle hide the field such that there is no conflict with current laboratory, solar system or cosmological experiments [1, 3]. Importantly, the chameleon mechanism is strong enough in such theories to allow strongly coupled theories with  $M \ll M_{Pl}$  to have remained thus far undetected [2].

The first term in the potential,  $V$ , corresponds to an effective cosmological constant whilst the second term is a Ratra-Peebles inverse power law potential. If one assumes that  $\phi$  is also responsible for late-time acceleration of the universe then one must require  $\Lambda \approx 2.3 \times 10^{-12} \text{ GeV}$ .

The evolution of the chameleon field in the presence of both matter and an external magnetic field is determined by the effective potential:

$$V_{\text{eff}}(\phi) = V(\phi) + \rho_{\text{eff}} e^{\phi/M} \quad (6)$$

where

$$\rho_{\text{eff}} = \rho_{\text{matter}} + \frac{B^2}{2} \quad (7)$$

and  $B$  is the magnetic field. As a result, even though  $V$  has a runaway form, the effective potential has a minimum at  $\phi = \phi_{\text{min}}(\rho_{\text{eff}})$  where

$$V'_{\text{eff}}(\phi_{\text{min}}) = 0 = V'(\phi_{\text{min}}) + \frac{1}{M} \left( \rho_{\text{matter}} + \frac{B^2}{2} \right). \quad (8)$$

In the presence of ambient matter and a magnetic field, the field evolves towards this minimum. The mass of small perturbations in  $\phi$  about  $\phi_{\text{min}}$  is given by

$$m_{\phi}(\phi_{\text{min}}) = \left( n(n+1) \frac{\Lambda^{n+4}}{\phi_{\text{min}}^{n+2}} \right)^{1/2}, \quad (9)$$

and we have that

$$\phi_{\text{min}} = \left( \frac{2n\Lambda^{4+n}M}{2\rho_{\text{matter}} + B^2} \right)^{1/(1+n)}. \quad (10)$$

In some circumstances, however,  $\phi$  is unable to change quickly enough to actually reach  $\phi_{\text{min}}$ . In particular, this behaviour can occur inside a low density cavity. If the radius,  $R$ , of the cavity is too small, then  $\phi$  does not reach its effective minimum and instead, as we show in Section III,  $m_{\phi} \sim 2/R$  for  $R \ll 2/m_{\phi}(\phi_{\text{min}})$ . Since laboratory searches for vacuum magnetic dichroism and birefringence generally employ such a cavity, one must be particularly wary of this behaviour when making predictions for what such experiments should detect. In particular the dependence of  $m_{\phi}$  on  $B$  and  $\rho_{\text{matter}}$  inside the experiment depends on the details of the set-up.

The chameleon mass,  $m_{\phi}$ , depends therefore on a number of factors. In searches for dichroism and birefringence in a vacuum, the mass depends on the details of the experimental set-up itself: the size of the cavity, the magnetic field  $B$  and the density of matter in the laboratory vacuum. The mass is *not* a fundamental parameter; the fundamental parameters of our model are  $\Lambda$ ,  $M$  and  $n$ . It is also important to note that, not only is  $m_{\phi}$  not a fundamental parameter, but that it is generally very different in different parts of experiments. We discuss the behaviour of  $m_{\phi}$  in laboratory searches for axion-like-particles (ALPs) in the next section.

### III. THE CHAMELEON MASS IN THE LABORATORY

In laboratory searches, such as the PVLAS [6], and Q&A [24] experiments, for the dichroism and birefringence induced by a magnetic field, light propagates in a Fabry-Perot cavity with radius  $R$ . The interaction region, i.e. the region where the magnetic field is turned on ( $B \neq 0$ ), has length  $L$ . To increase the strength of any signal the light is reflected  $N$  times, and the mirrors are located a distance  $d$  from either end of the interaction region. We label the density of the vacuum matter inside the cavity by  $\rho_{\text{gas}}$ . For example in the PVLAS experiment  $L = 100 \text{ cm}$ ,  $d = 270 \text{ cm}$ ,  $R = 12.5 \text{ mm}$  and  $\rho_{\text{gas}} \approx 2 \times 10^{-4} \text{ g cm}^{-3}$ . Before we can make predictions for the dichroism and birefringence we need to know the value of  $m_{\phi}$  along the path of the photon. Although we are primarily concerned with power-law type potentials, in most of the discussion in this section we do not assume any particular form of  $V$ , we only require that it satisfies the chameleon field theory conditions given by Eq. (4).

The cavity is a cylinder with radius  $R$ . Outside of the cavity (i.e. in the walls of the cavity and the surrounding magnet),  $\phi$  must lie close to its effective minimum, which we label by  $\phi = \phi_{\infty}$ . If this were not the case then the walls

of two such cavities would feel a force that would be  $2(M_{Pl}/M)^2 \gg 1$  times their gravitational attraction. Such a force is easily ruled out by experimental tests of gravity. We define  $r$  to be the radial distance from the centre of the cavity and define  $\phi_0 = \phi(r=0)$ . We approximate the potential inside and outside the cavity as a quadratic function. Outside the cavity, the expansion is around the minimum where  $V'_{\text{eff}}(\phi_\infty) = 0$ . Inside we expand around  $\phi_0$  which is left unknown. This leads to two equations for the field  $\phi$ . For  $r \geq R$  we have

$$\phi'' + \frac{1}{r}\phi' - m_\infty^2(\phi - \phi_\infty) = 0, \quad (11)$$

whereas for  $r \leq R$  the equation reads

$$\phi'' + \frac{1}{r}\phi' - m_0^2(\phi - \phi_0) = V'_{\text{eff}0}, \quad (12)$$

where  $V'_{\text{eff}0} = V'(\phi_0) + \rho_{\text{eff}}e^{\phi_0/M}$ . Note that in most cases  $\phi_0$  is not  $\phi_c$  where  $V'_{\text{eff}}(\phi_c) = 0$ . We define  $V'_c = V'(\phi_c)$  and  $V'_0 = V'(\phi_0)$ , we can then write  $V'_{\text{eff}0} = V'_0 - V'_c$ .

The non-singular solution for  $r \leq R$  is a combination of the Bessel functions  $J_0$  and  $N_0$ . However, since  $N_0$  diverges logarithmically at the origin, we ignore the term containing  $N_0$  and therefore the solution inside the cavity reads

$$\phi = CJ_0(im_0r) + \phi_0 - \frac{V'_0 - V'_c}{m_0^2}. \quad (13)$$

On the other hand, for  $r \geq R$ , the solution is

$$\phi = A(J_0(im_\infty r) - iN_0(im_\infty r)) + \phi_\infty \quad (14)$$

Matching both solutions and their first derivatives at  $r = R$  gives the following conditions for  $A$  and  $C$ :

$$A = \frac{m_0 J'_0(im_0 R)(\phi_\infty - \phi_0 + (V'_0 - V'_c)/m_0^2)}{m_\infty J_0(im_0 R)(J'_0 - iN'_0)(im_\infty R) - m_0 J'_0(im_\infty R)(J_0 - iN_0)(im_\infty R)},$$

and

$$C = \frac{m_\infty (J'_0 - iN'_0)(im_\infty R)}{m_0 J'_0(im_0 R)} A.$$

Now, since  $\phi$  must lie very close the effective minimum inside the cavity walls, we must have

$$m_\infty R \gg 1.$$

The solution inside the cavity then simplifies drastically

$$\phi = \frac{\phi_\infty - \phi_0 + \frac{V'_0 - V'_c}{m_0^2}}{J_0(im_0 R)} J_0(im_0 r) + \phi_0 - \frac{V'_0 - V'_c}{m_0^2}. \quad (15)$$

Evaluating this equation at  $r = 0$  and imposing  $\phi(r=0) = \phi_0$  leads to

$$\phi_\infty - \phi_0 = \frac{V'_0 - V'_c}{m_0^2} (J_0(im_0 R) - 1) \quad (16)$$

There are now two relevant situations:

#### A. $m_c R \gg 1$

Since  $m_0 \leq m_c$ ,  $m_0 R \gg 1$  in this case. It follows from Eq. (16) that  $V'_0 \approx V'_c$  and therefore that  $m_0 \approx m_c$ .

### B. $m_c R \ll 1$

If  $V'_0/V'_c - 1 \lesssim \mathcal{O}(1)$  that would require  $m_0 \approx m_c$  and by the matching condition  $m_0 R \approx m_c R \gtrsim \mathcal{O}(1)$ . If  $m_c R \ll 1$  we must therefore have  $V'_0/V'_c - 1 \gg 1$ , and so

$$1 + J_0(im_0 R) = \frac{m_0^2(\phi_0 - \phi_\infty)}{|V'_0|}.$$

The right hand side of this equation is generally  $\mathcal{O}(1)$  or smaller and so  $m_0 R = \mathcal{O}(1)$  which implies  $m_0 \ll m_\infty$  and  $\phi_\infty \ll \phi_0$  due to the runaway form of the potential. For the inverse power-law potential  $V'_0/m_0^2 = -\phi_0/(n+1)$ , and the matching equation therefore gives

$$J_0(im_0 R) = n + 2, \tag{17}$$

which implies, as expected, that  $m_0 R = \mathcal{O}(1)$  for  $n = \mathcal{O}(1)$ . Expanding the Bessel function for small  $m_0 R \ll 4$  in the last equation gives

$$m_0 R \approx 2\sqrt{n+1}. \tag{18}$$

A slightly better approximation for  $\mathcal{O}(1)$  values of  $n$  is given by:

$$m_0 R \approx 2\sqrt{2}(\sqrt{n+2} - 1)^{1/2}. \tag{19}$$

Note that if  $m_c R \sim \mathcal{O}(1)$  then we could not ignore the  $V'_c$  term in the matching condition, but since  $V'_c < 0$  we would have:

$$J(im_0 R) - 1 > n + 2,$$

and so  $m_0 R$  is *always* larger than the value defined by Eq. (17). In summary: we have found that there are two relevant cases for the chameleon mass. In the first case, the length scale set by the chameleon mass inside the cavity ( $1/m_0$ ) is much smaller than the size of the experiment. In the second case, the length scale  $1/m_0$  is  $\mathcal{O}(R)$ , and we found an approximate relation Eq. (17) between the mass inside the cavity,  $R$  and the properties of the potential, encoded here in the power  $n$ . Eq. (17) also defines the smallest possible value of  $m_0$ . It is clear that for  $\mathcal{O}(1)$  values of  $n+1$  we *cannot* have  $m_0 \ll 1/R$ .

## IV. CHAMELEON OPTICS IN A CAVITY

It was shown in Ref. [5] that to avoid constraints on solar ALP production from the CAST experiment, one must require that in bodies with densities of the order of  $10 \text{ g cm}^{-3}$  the chameleon mass satisfies  $m_\phi \geq 10^4 \text{ eV}$ . In experiments such as BRFT, PVLAS, and Q&A the photon beam typically has a frequency  $\omega = \mathcal{O}(1) \text{ eV}$ . In the mirrors then  $m_\phi \gg \omega$  and so the chameleon field cannot escape the cavity. Indeed the propagation of the chameleon field outside the cavity is exponentially attenuated implying that the cavity mirrors also act as perfect mirrors for the chameleon field. This is at odds with the usual assumption that ALPs escape from the cavity without any reflection. The standard expressions for the rotation (dichroism) and the ellipticity (birefringence) must therefore be modified.

In this section we study the propagation of a beam of light in the presence of a chameleon field and derive expressions for the predicted rotation and ellipticity. For simplicity we initially assume that there is no distance between the end of the interaction region and the mirrors, and that the chameleon and photon fields reflect in the same way. Whilst neither of these assumptions are generally true, and there are important effects associated with the violation of each of them, the calculation is much simpler and easy to follow if we make them. We say more about what occurs when these assumptions are dropped in subsection IV D below.

We assume that the scalar field mixes with the orthogonal polarization to the magnetic field. This system is a two-level system with two states  $|P\rangle$  and  $|S\rangle$  for the photon and the scalar in the absence of the magnetic field. For the system of differential equations satisfied by the photon and the scalar, see the Appendices. When a magnetic field is turned on, the two states mix and the eigenstates are

$$\begin{aligned} |+\rangle &= \cos\theta|S\rangle + i\sin\theta|P\rangle \\ |-\rangle &= \cos\theta|P\rangle + i\sin\theta|S\rangle \end{aligned}$$

where

$$\tan 2\theta = \frac{2B\omega}{Mm^2} \quad (20)$$

The eigenvalues for the above system are given by

$$k_{\pm}^2 = \omega^2 - m^2 \frac{\cos 2\theta \pm 1}{2 \cos 2\theta}. \quad (21)$$

For small  $\theta$  we get

$$k_+ = \omega^2 - m^2 \left(1 + \frac{\theta^2}{2}\right) \quad (22)$$

and

$$k_-^2 = \omega^2 + m^2\theta^2 \quad (23)$$

In particular we find

$$k_+ = \omega - \frac{m^2}{2\omega} \quad (24)$$

and

$$k_- = \omega + \frac{m^2\theta^2}{2\omega}, \quad (25)$$

which is crucial in the following.

### A. Free propagation

We consider first the situation where the electromagnetic wave and the chameleon propagate freely. Assuming that the state at a given origin is  $|P\rangle$  ( $z=0$ ), then state at a further position  $z$  is given by

$$|P\rangle(z) = \cos k_- z \cos \theta |-\rangle - i \cos k_+ z \sin \theta |+\rangle \quad (26)$$

This mixed state can be expressed in terms of the free scalar and photon as

$$|P\rangle(z) = (\cos^2 \theta \cos k_- z + \sin^2 \theta \cos k_+ z) |P\rangle + i \sin \theta \cos \theta (\cos k_- z - \cos k_+ z) |S\rangle$$

The photon part for small  $\theta$  and using the expansion of  $k_{\pm}$  (24,25), is given by

$$\psi(z) = \left(1 - 2\theta^2 \sin^2 \frac{m^2 z}{4\omega}\right) \cos \left(\omega z + \frac{m^2 \theta^2}{2\omega} z - \theta^2 \sin \frac{m^2 z}{2\omega}\right), \quad (27)$$

from which we identify the attenuation and the phase shift

$$a = 2\theta^2 \sin^2 \frac{m^2 z}{4\omega}, \quad \delta = \frac{m^2 \theta^2}{2\omega} z - \theta^2 \sin \frac{m^2 z}{2\omega} \quad (28)$$

From those, dividing by two, one gets the rotation and the ellipticity for an incoming laser beam with a 45 degree polarization. We finish the subsection defining a quantity which will be very useful below

$$z_{\text{coh}} = \frac{2\omega}{m^2}, \quad (29)$$

measuring the coherence of the system.

## B. Propagation in a cavity

The only difference between the free propagation case and a propagation within a cavity of size  $L$  is that we need to sum over periodic copies shifted by  $nL$ . The mirrors are not perfect, so only  $N < \infty$  passes actually occur. Mathematically, this system is equivalent to the coupled wave equations in a periodic box.

Let us define first

$$a_n(z) = 2\theta^2 \sin^2 \frac{m^2(z + nL)}{4\omega} \quad (30)$$

and

$$\delta_n(z) = \frac{m^2\theta^2}{2\omega}(z + nL) - \theta^2 \sin \frac{m^2(z + nL)}{2\omega} \quad (31)$$

The photon wave function is then given by summing

$$\psi(z) = \sum_{n=0}^{N-1} (1 - a_n) \cos k_-(z + nL) + \theta^2 \sin \frac{m^2(z + nL)}{2\omega} \sin k_-(z + nL) \quad (32)$$

In a perfect cavity, the waves have a resonance, i.e.  $\omega L = 2\pi p$ . Therefore

$$\begin{aligned} \psi(z) = & \sum_{n=0}^{N-1} (1 - a_n) \cos \left( \omega z + \frac{m^2\theta^2}{2\omega}(z + nL) \right) \\ & + \theta^2 \sin \frac{m^2(z + nL)}{2\omega} \sin k_-(z + nL) \end{aligned} \quad (33)$$

Using the small  $\theta$  approximation, one obtains

$$\begin{aligned} \psi(z) = & N \left( 1 - \frac{1}{N} \sum_{n=0}^{N-1} a_n \right) \cos \omega z \\ & + \sum_{n=0}^{N-1} \left( \theta^2 \sin \frac{m^2(z + nL)}{2\omega} - \frac{m^2\theta^2}{2\omega}(z + nL) \right) \sin \omega z \end{aligned} \quad (34)$$

Notice this is nothing but a standing wave

$$\psi(z) = N \left( 1 - \frac{1}{N} \sum_{n=0}^{N-1} a_n(z) \right) \cos \left( \omega z + \frac{1}{N} \sum_{n=0}^{N-1} \delta_n(z) \right) \quad (35)$$

So the phase shift and the attenuation at the end of the cavity  $z = L$  are given by

$$\delta_T = \frac{1}{N} \sum_{n=0}^{N-1} \delta_n(L), \quad a_T = \frac{1}{N} \sum_{n=0}^{N-1} a_n(L) \quad (36)$$

These sums can be exactly computed, which give

$$\delta_T = \theta^2 \left( \frac{(N+1)L}{2z_{\text{coh}}} + \frac{\sin N \frac{L}{z_{\text{coh}}} + \sin \frac{L}{z_{\text{coh}}} - \sin(N+1) \frac{L}{z_{\text{coh}}}}{2N(1 - \cos \frac{L}{z_{\text{coh}}})} \right) \quad (37)$$

For larger values and using  $\sin x \leq x$ , we have the inequality  $\delta_T \leq \delta_N$ .

Similarly the attenuation is

$$a_T = \theta^2 \left( 1 - \frac{1 + \cos N \frac{L}{z_{\text{coh}}} - \cos \frac{L}{z_{\text{coh}}} - \cos(N+1) \frac{L}{z_{\text{coh}}}}{2N(1 - \cos \frac{L}{z_{\text{coh}}})} \right). \quad (38)$$

### C. Coherence

The previous expressions can be easily interpreted in terms of the coherence of the photon-scalar system. We focus on the case where the coherence length and the length of the experiment are commensurate. Define the number of coherent passes as  $PL = 2\pi z_{\text{coh}}$ . Using this one finds that

$$a_{n+P} = a_n, \quad \delta_{n+P} = \delta_n + \frac{m^2\theta^2}{2\omega}PL \quad (39)$$

The attenuation is then given by

$$a_T = \frac{1}{N} \sum_{j=0}^{N/P-1} \sum_{n=0}^{P-1} a_{n+jP} = \frac{1}{N} \sum_{j=0}^{N/P-1} \sum_{n=0}^{P-1} a_n \quad (40)$$

and therefore

$$a_T = \frac{1}{P} \sum_{n=0}^{P-1} a_n \quad (41)$$

Hence the attenuation depends only on the coherence length, after  $P$  passes, the waves are not coherent any more. Using the previous formulae we find

$$a_T = \theta^2 \quad (42)$$

and for the rotation

$$\text{rotation/pass} = \frac{\theta^2}{2N} \quad (43)$$

which was first derived in [26].

In order to get the ellipticity one notes first that the phase shift is given by

$$\delta_T = \frac{1}{N} \sum_{j=0}^{N/P-1} \sum_{n=0}^{P-1} \delta_{n+jP} = \frac{1}{N} \sum_{j=0}^{N/P-1} \sum_{n=0}^{P-1} \left( \delta_n + jPL \frac{m^2\theta^2}{2\omega} \right) \quad (44)$$

and therefore

$$\delta_T = PL \left( \frac{N}{P} - 1 \right) \frac{m^2\theta^2}{4\omega} + (P+1)\theta^2 \frac{L}{2z_{\text{coh}}} \quad (45)$$

Using the definition of  $P$  one finds

$$\delta_T = \pi \left( \frac{N}{P} - 1 \right) \theta^2 + 2\pi \frac{P+1}{P} \theta^2 \quad (46)$$

For large  $P$  this simplifies to

$$\delta_T = \pi \left( \frac{N}{P} - 1 \right) \theta^2 \quad (47)$$

This can also be written for  $N/P \gg 1$  as

$$\delta_T = \frac{NLm^2}{4\omega} \theta^2 \quad (48)$$

Which again was found in [26]. The ellipticity per pass is now

$$\text{ellipticity/pass} = \frac{\pi\theta^2}{2} \left( \frac{1}{P} - \frac{1}{N} \right) \quad (49)$$

and one finds that the ellipticity per rotation is

$$\frac{\text{ellipticity}}{\text{rotation}} = \pi \left( \frac{N}{P} - 1 \right) = \pi \left( \frac{NL}{2\pi z_{\text{coh}}} - 1 \right) \quad (50)$$

In particular, for large  $N$ , the ellipticity is always much larger than the rotation. This fact is still true when the non-interacting zone of length  $d$  is taken into account. It is a crucial prediction of chameleon theories.



### D. Phase Shifts

The above calculation has been performed under the assumptions that there is no gap between the ends of the interaction region and the mirrors and that the chameleon field reflects off the mirror in precisely the same way as the photon does. Unfortunately, neither of these assumptions are generally true.

In the PVLAS, BRFT and Q&A experiments, there is always some gap between the end of the interaction region and the mirrors. In PVLAS this gap is 270 cm long. Outside the interaction region both the chameleon field and the photon field propagate freely, however since the chameleon field is massive it travels more slowly than the photon. As we show in Appendix B, this leads to the chameleon field picking up a phase shift  $\Delta_m$  relative to the photon field when the field returns to the interaction region. This phase shift alters the formulae for the rotation and ellipticity. We find that if there is a distance  $d$  between the mirror outside the interaction region, then  $\Delta_m \approx m_\phi^2 d/\omega$ . In addition

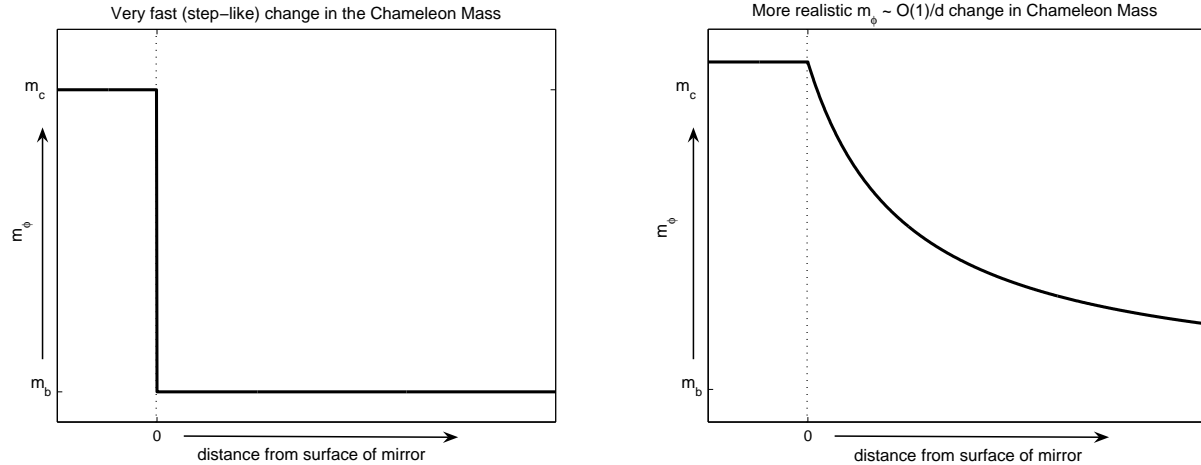


FIG. 1: Illustration of the difference between a sharp (step-like) change in the chameleon mass at the surface of the mirror and the more realistic  $m_\phi \sim \mathcal{O}(1/d)$ , for  $d \gg 1/m_c$ , behaviour, where  $d$  is the distance from the surface of the mirror. In both of these sketches,  $m_c$  is the chameleon mass inside the mirror and  $m_b$  is the chameleon mass far from the mirror. The dotted line indicates the surface of the mirror.

to the phase shift  $\Delta_m$ , there is generally an additional phase shift  $\Delta_r$  due to the manner in which the chameleon field reflects off the mirror. Consider a mirror placed at  $x = 0$ . If  $m_\phi$  behaved like a step function, see Figure 1, where  $m_\phi = m_<$  for  $x < 0$  and  $m_\phi = m_>$  for  $x > 0$  and  $m_> \ll m_<$ , then the wave function of a chameleon wave with wave-number  $k$  incident on the mirror would, in  $x > 0$ , have the form:

$$\delta\phi \approx \delta\phi_0 \sin(kx).$$

When  $x < 0$ ,  $\phi$  decays away exponentially. However, in realistic theories  $\phi$  is continuous across  $x = 0$  and so  $m_\phi$  is too. Indeed, in Appendix B, we show, via a similar calculation to the one performed in Section III above, that for  $1/m_< \lesssim x \lesssim 1/m_>$  we have  $m_\phi \approx \mathcal{O}(1/x)$  (see Figure 1).

It should be noted that this behaviour is not specific to the inverse power-law potentials considered here, but is generic to almost all chameleon theories (see Appendix B for a complete discussion). A scalar wave with frequency  $\omega$  switches from oscillatory to exponentially decaying behaviour when  $m_\phi^2 = \omega^2$ . In chameleon theories this transition therefore occurs at a distance  $x_r = \mathcal{O}(1/\omega)$  from the mirror. Chameleon waves therefore behave as if they reflect not at  $x = 0$  but at  $x = x_r > 0$ . Schematically this alters the form of the chameleon wave function in  $x > x_r$  to:

$$\delta\phi \approx \delta\phi_0 \sin(k(x - x_r)).$$

As is shown in Appendix B, this early reflection produces another phase shift,  $\Delta_r$ , in the chameleon wave relative to the photon wave when they return to the interaction region. We find that for inverse square law potentials:

$$\Delta_r = \frac{\pi n}{n + 2},$$

where  $n > 0$ .

The presence of a total phase shift  $\Delta \approx \Delta_r + \Delta_m$  alters the formulae for the rotation,  $\Delta\varphi$  and ellipticity,  $\psi$  and these are calculated in Appendix A. Both of the mentioned effects will exist, to some degree in all theories in which the ALP does not escape the cavity. We find that when  $\Delta \neq 0$  and provided that:

$$\left( \frac{B\omega \sin\left(m_\phi^2 L/4\omega\right)}{Mm_\phi^2 \sin\left(\Delta/2 + m_\phi^2 L/4\omega\right)} \right)^2 \ll 1, \quad (51)$$

we predict

$$\begin{aligned} \frac{\Delta\varphi}{\sin 2\varphi} = & - \left( \frac{B\omega}{Mm_\phi^2} \right)^2 H_\Delta \left( \frac{m_\phi^2 L}{2\omega} \right) \left\{ \frac{1}{2} + \left[ \sin^2 \left( \frac{N\Delta}{2} + \frac{Nm_\phi^2 L}{4\omega} \right) \right. \right. \\ & \left. \left. - \frac{1}{2} \right] \delta_N \left( \Delta + \frac{m_\phi^2 L}{2\omega} \right) \right\}, \end{aligned} \quad (52)$$

and

$$\begin{aligned} \frac{\psi}{\sin 2\varphi} = & - \frac{1}{2} \left( \frac{B\omega}{Mm_\phi^2} \right)^2 \left\{ \frac{Nm_\phi^2 L}{2\omega} - NG_\Delta \left( \frac{m_\phi^2 L}{2\omega} \right) \right. \\ & \left. - \sin \left( N\Delta + \frac{Nm_\phi^2 L}{2\omega} \right) H_\Delta \left( \frac{m_\phi^2 L}{2\omega} \right) \delta_N \left( \Delta + \frac{m_\phi^2 L}{2\omega} \right) \right\}. \end{aligned} \quad (53)$$

where

$$G_\Delta(x) = \frac{2 \sin(\Delta/2) \sin(x/2)}{\sin(\Delta/2 + x/2)}, \quad (54)$$

$$H_\Delta(x) = \frac{\sin^2(x/2)}{\sin^2(\Delta/2 + x/2)}, \quad (55)$$

and

$$\delta_N(x) = \frac{\sin((N+1)x)}{(N+1)\sin x}. \quad (56)$$

The phase  $\Delta$  is given by

$$\Delta = \frac{m_\phi^2 d}{\omega} + \Delta_r, \quad (57)$$

where  $\Delta_r$  depends on the potential  $V(\phi)$ . For inverse power-law potential ( $n > 0$ ),  $\Delta_r$  is given by

$$\Delta_r = \frac{\pi n}{n+2}. \quad (58)$$

When  $\Delta = 0$ ,  $G_\Delta = 0$  and  $H_\Delta = 1$ . We always have  $|\delta_N(x)| < 1$ , and for  $N$  large  $\delta_N(x)$  is strongly peaked about  $x = m\pi$  for any integer  $m$  and  $\delta_N(x) \ll 1$  otherwise. In many situations one finds that  $m_\phi^2(L/2 + d)/2\omega \ll 1$  and  $\tan(\Delta_r/2) \sim \mathcal{O}(1)$ . In these circumstances, the expressions for the ellipticity and rotation simply greatly:

$$\begin{aligned} \frac{\Delta\varphi}{\sin \varphi} & \approx \frac{B^2 L^2}{32M^2 \sin^2\left(\frac{\Delta_r}{2}\right)}, \\ \frac{\psi}{\sin \varphi} & \approx - \frac{NB^2 L^2}{16M^2 \tan\left(\frac{\Delta_r}{2}\right)}, \end{aligned}$$

which are both independent of  $m_\phi$ . In this limit, the ratio of the rotation to the ellipticity is:

$$\frac{\Delta\varphi}{\psi} = \frac{1}{N \sin(\Delta_r)}. \quad (59)$$

## V. PREDICTIONS

Having described the physics and derived the basic formulae for rotation and ellipticity induced by the coupling of a chameleon field to the electromagnetic sector, we now study the predictions of the chameleon model. To simplify the analysis, we have assumed that the chameleon couples to all matter types (including photons) with the same strength. In this case, there is a lower bound on the energy scale  $M$  coming from the contribution of the chameleon to the anomalous magnetic moment of the muon and electron. The contribution is of order  $(m_{e,\mu}/M)^2$  [27]. In order for the chameleon contribution to the anomalous magnetic moment of the muon to be small enough,  $M$  has to be bigger than  $M \approx 10^4$  GeV. We will therefore concentrate here on the case  $M > 10^4$  GeV. We should mention here that if the couplings differ from species to species, this constraint on the coupling to the electromagnetic sector could be relaxed.

The predictions for rotation and ellipticity are shown in Figure 2. One feature of the chameleon model is that the ellipticity is generally predicted to be much larger than the rotation. This can be viewed as a generic prediction of chameleon theories. In general, a large ellipticity to rotation ratio occurs (for large  $N$ ) whenever:

- The ALPs are reflected by the mirrors rather escaping through them.
- The ALPs from previous passes are not coherent with the photon field.

If the ALPs were to escape then each pass would give the same contribution to the rotation and ellipticity, these add up and thus both  $\Delta\varphi$  and  $\psi$  would be proportional to  $N$ . However, if the first of the above conditions is satisfied then this is not the case, since ALPs from previous passes interact with the photon field and thus the way in which the rotation and ellipticity build up is altered. If, additionally, ALPs from previous passes are *not* coherent with the photon field, then a large degree of cancellation of both the ellipticity and rotation occurs. For large  $N$ , the cancellation in the rotation,  $\Delta\varphi$ , is almost exact, and as result  $\Delta\varphi$  is almost independent of  $N$ .

Cancellation of contributions to the ellipticity also occurs. However, there is always at least one contribution which does not cancel but builds up as the number of passes increases. This contribution results from the fact that the component of the photon field that interacts with the ALP propagates more slowly in the interaction region than its non-interacting component. As a result the relative phase of the interacting and non-interacting components is shifted. This contribution to the ellipticity is unaffected by the decoherent ALPs. There is, therefore, always at least one contribution to the ellipticity that is proportional to  $N$ . Thus the combination of reflecting ALPs and their becoming decoherent results in the ellipticity but not the rotation growing as  $N$ . The rotation to ellipticity ratio is therefore  $\sim 1/N \ll 1$  (see Eq. (59) for a better estimate).

If the ALP in question is a chameleon field then both reflection and decoherence almost certainly occur. Reflection occurs because the mass of the chameleon inside the mirror,  $m_c$ , is much larger than the mass far outside,  $m_b$ , and the energy of beam,  $\omega$ , used in experiments is almost always  $\ll m_c$ . Decoherence occurs because, as we found in Appendix B, at a distance  $x$  ( $1/m_c \ll x \ll 1/m_b$ ) from the surface of the mirror, the chameleon mass behaves as  $\sim \mathcal{O}(1)/x$ . The reflection of the chameleon does not, therefore, occur on the surface of the mirror but a distance  $x_r \sim \mathcal{O}(1)/\omega$  from the mirror's surface. This, we found, resulted in an  $\mathcal{O}(1)$  phase shift between the reflected chameleon and photon fields. Generally then, the chameleon fields from previous passes are both reflected and are not coherent with the photon field. Whilst, one could probably construct a chameleon theory where one or both of the above conditions did not hold, it would not be particularly generic and might also have problems satisfying gravitational and other laboratory constraints on such theories.

It is therefore a generic feature of chameleon theories that the rotation to ellipticity ratio is  $O(1/N) \ll 1$ . This means that, according to the chameleon model, it is easier to detect the ellipticity than the rotation.

In Section III we showed how, for a given experimental set-up and choice of  $V(\phi)$ , the chameleon mass,  $m_\phi$ , in the interaction could be calculated from the chameleon-to-matter coupling if  $\Lambda$  and  $n$  are known. We found that there were two regimes. If the density of the vacuum,  $\rho_{\text{gas}}$ , and the radius,  $R$ , of the cavity were small enough and  $M$  large enough then  $m_\phi \sim \mathcal{O}(2)/R$  for small  $n$ . Alternatively, if  $M$  is small enough or  $\rho_{\text{gas}}/R$  large enough, then the chameleon mass depends on  $(\rho_{\text{gas}} + B^2/2)/M$ . The chameleon mass and therefore the predicted ellipticity and rotation are therefore highly dependent on the set-up of the axion search experiment. In the chameleon model, there is no reason to expect that two different experiments should detect the same ellipticity and rotation.

### A. Predictions for PVLAS, Q&A, BMV and BRFT

As we argued in Section II, we expect  $\Lambda \approx 2.3 \times 10^{-3}$  eV if the energy density of the chameleon field is to be associated with dark energy. Ideally, one would determine both  $\Lambda$  and  $n$  from an experimental detection. However, since the status of the only (i.e. PVLAS) detection reported to date is unclear, we now consider the specific predictions

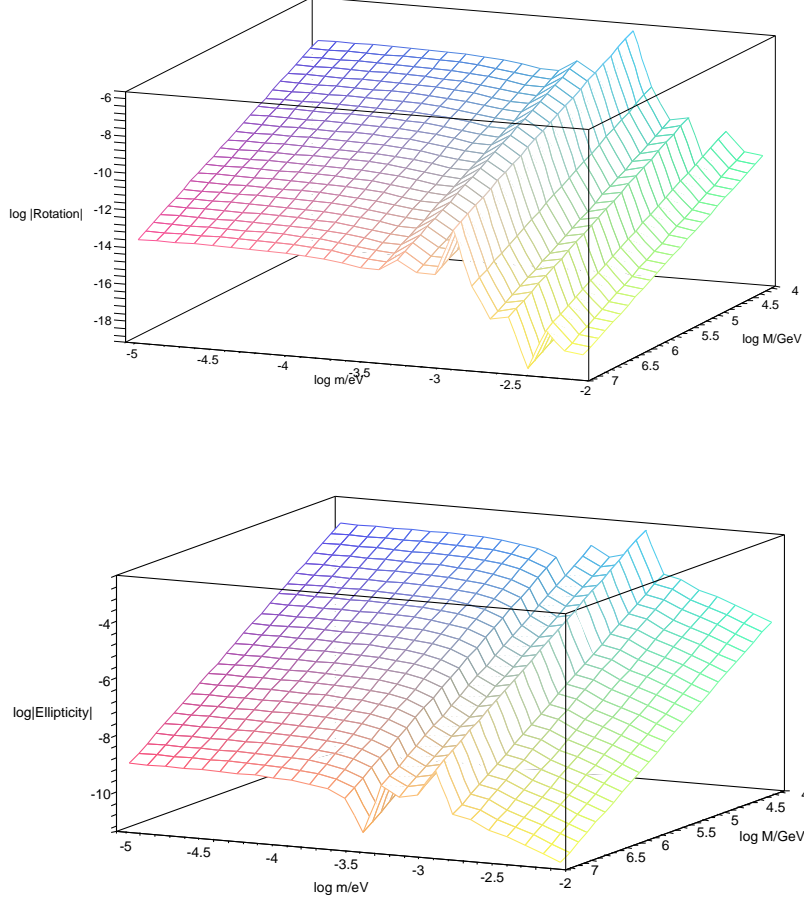


FIG. 2: Predictions for rotation (upper plot) and ellipticity (lower plot) in the chameleon model as a function of  $M$  and  $m_\phi$ . The PVLAS set-up is used ( $L = 100$  cm,  $d = 270$  cm,  $\omega = 1.2$  eV,  $B = 5$  T and  $\varphi = \pi/4$ ). Furthermore we have chosen  $n = 1$ .

for the chameleon model for  $\Lambda \approx 2.3 \times 10^{-3}$  eV and  $n = 1$ . The vacuum used in the PVLAS set-up is very good, with a density of about  $2 \times 10^{-14}$  gcm $^{-3}$ , whereas the density of the Q&A experiment's vacuum is significantly higher:  $8.5 \times 10^{-9}$  gcm $^{-3}$ ; as a result, for  $M \sim 10^6 - 10^{10}$  GeV, the chameleon mass in the PVLAS experiment  $\sim \mathcal{O}(2)/R$  and hence independent of  $M$ . In the Q&A experiment, however,  $m_\phi$  is, for given  $M$ , both larger than it is in the PVLAS set-up and depends on  $(\rho_{\text{gas}} + B^2/2)/M$ . The larger value of  $m_\phi$  in the Q&A set-up means that the ellipticity and rotation predicted by the chameleon model are far smaller than those predicted for the PVLAS experiment. The chameleon model predictions for both the PVLAS and Q&A set-up are shown in Figure 3. The thin dotted lines in these plots show the 2.3 T PVLAS 2007 [10] and Q&A 95% confidence limits on the rotation and ellipticity. For  $M > 10^4$  GeV it is only the 2.3 T PVLAS upper bound on the ellipticity that provides a useful constraint on  $M$ : we must require  $M \gtrsim 2 \times 10^6$  GeV if  $n = 1$  and  $\Lambda \approx 2.3 \times 10^{-3}$  eV. A similar limit of  $M$  is found for other values of  $n$ .

The PVLAS experiment performs better than Q&A as a probe for chameleon fields because of the high quality vacuum it employs. The upcoming BMV experiment uses a similar high quality vacuum with pressure  $< 10^{-8}$  mbar [29, 30]. This experiment will additionally use a higher strength magnetic field than PVLAS, employ a greater number of passes and additionally promises a higher precision. Figure 4 shows the predicted rotation and ellipticity signals for PVLAS (with both  $B = 2.3$  T and 5.5 T) and BMV again with  $n = 1$  and  $\Lambda = 2.3 \times 10^{-3}$  eV. We see that BMV should be able to detect, or rule out, such chameleon theories with  $M \lesssim 3 \times 10^7$  GeV which represents an order of magnitude improvement over PVLAS.

For completeness, we show in Figure 5 the predicted rotation and ellipticity signals for PVLAS ( $B = 2.3$  T) and BRFT (for two different number of passes  $N$ ) again with  $n = 1$  and  $\Lambda = 2.3 \times 10^{-3}$  eV. Notice that, although chameleon models predict a higher rotation and ellipticity within the BRFT set up, we see that BRFT should only be able to detect, or rule out, such chameleon theories with  $M \lesssim 8 \times 10^5$  GeV. This is worse than that provided by

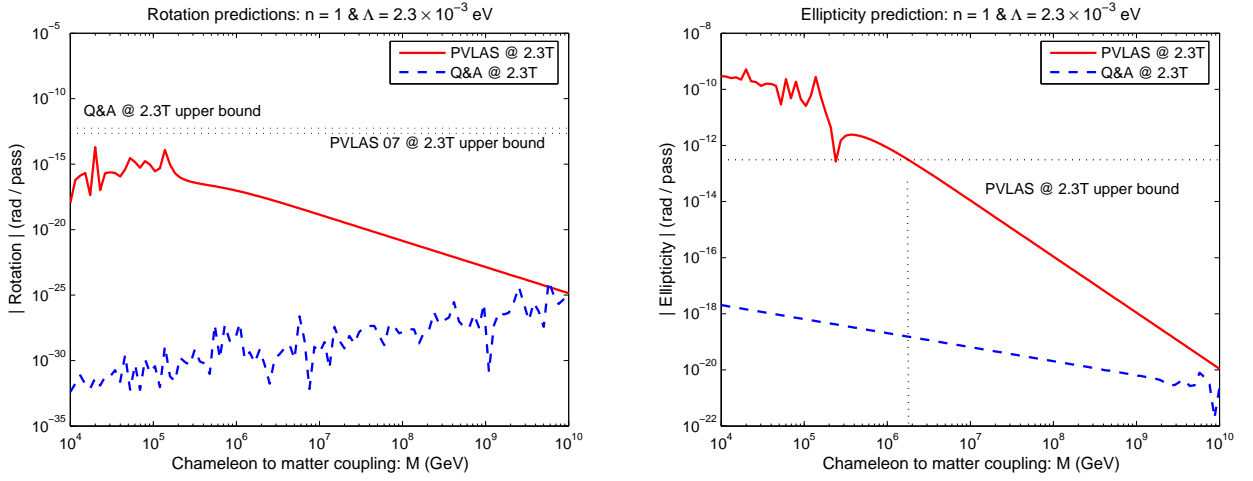


FIG. 3: Predictions for rotation (left) and ellipticity (right) in the chameleon model as a function of  $M$  for  $\Lambda = 2.3 \times 10^{-3}$  eV and  $n = 1$ . Predictions for the 2.3 T PVLAS ( $L = 100$  cm,  $d = 270$  cm,  $\omega = 1.2$  eV,  $B = 2.3$  T,  $\rho_{\text{gas}} = 2 \times 10^{-14}$  gcm $^{-3}$  and  $\varphi = \pi/4$ ) and Q&A ( $L = 60$  cm,  $d = 145$  cm,  $\omega = 1.2$  eV,  $B = 2.3$  T,  $\rho_{\text{gas}} = 8.5 \times 10^{-9}$  gcm $^{-3}$  and  $\varphi = \pi/4$ ) set-ups are shown. The thin-dotted lines show the 95% confidence upper bounds on both the rotation and the ellipticity.

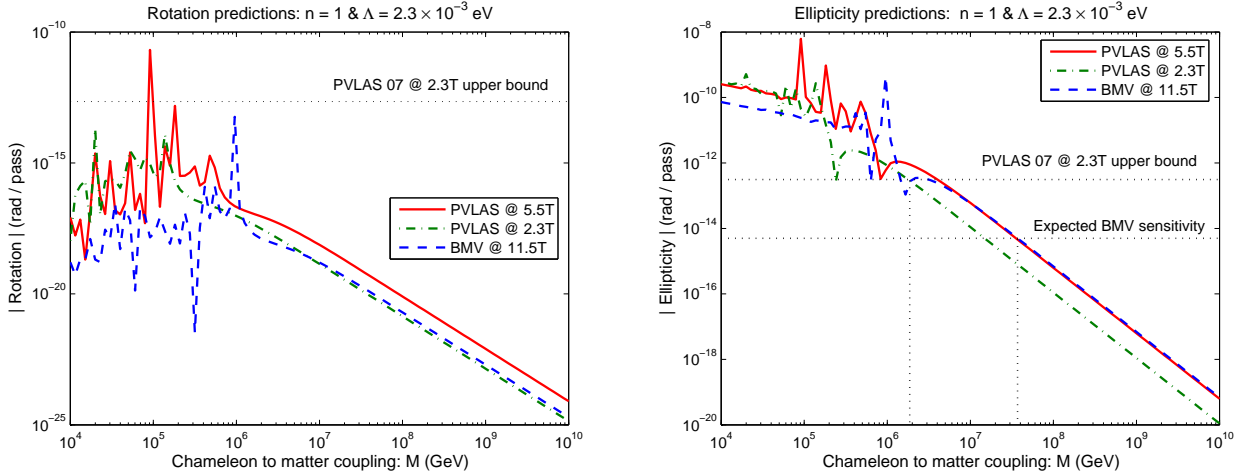


FIG. 4: Predictions for rotation (left) and ellipticity (right) in the chameleon model as a function of  $M$  for  $\Lambda = 2.3 \times 10^{-3}$  eV and  $n = 1$ . Predictions for the  $B = 2.3$  T and  $B = 5.5$  T PVLAS ( $L = 100$  cm,  $d = 270$  cm,  $\omega = 1.2$  eV,  $\rho_{\text{gas}} = 2 \times 10^{-14}$  gcm $^{-3}$  and  $\varphi = \pi/4$ ) and BMV ( $L = 50$  cm,  $d = 85$  cm,  $\omega = 1.2$  eV,  $B = 11.5$  T,  $\rho_{\text{gas}} \approx 10^{-14}$  gcm $^{-3}$  and  $\varphi = \pi/4$ ) set-ups are shown. The thin-dotted lines show the 95% confidence upper bounds on both the rotation and the ellipticity.

PVLAS. Even though the BRFT and PVLAS set-ups use vacuums of similar quality, the smaller number of passes in the BRFT experiment result in it placing a much weaker bound on the ellipticity per pass than the PVLAS bound.

## B. Dependence of predictions on $n$

In Figures 2-4 we took  $n = 1$ . Theories with different values of  $n$  do, however, lead to different predictions. Figure 6 shows how the ellipticity and rotation predicted for the PVLAS set-up depend on  $n$ . We found above that if  $X = m_\phi^2(d + L/2)/2\omega \ll 1$  and  $\tan(\Delta_r/2) \sim \mathcal{O}(1)$  then:

$$\psi \approx -\frac{B^2 L^2 N}{16M^2 \tan(\Delta_r(n)/2)}(1 + \mathcal{O}(X)) \approx N \sin(\Delta) \Delta \varphi,$$

which depends on  $n$  only through  $\Delta_r(n) = \pi n/(n + 2)$ . Thus for values of  $M$  such that  $X \ll 1$ , which for PVLAS roughly corresponds to  $M \gg 10^6$  GeV, both the ellipticity and rotation are therefore only very slightly dependent on

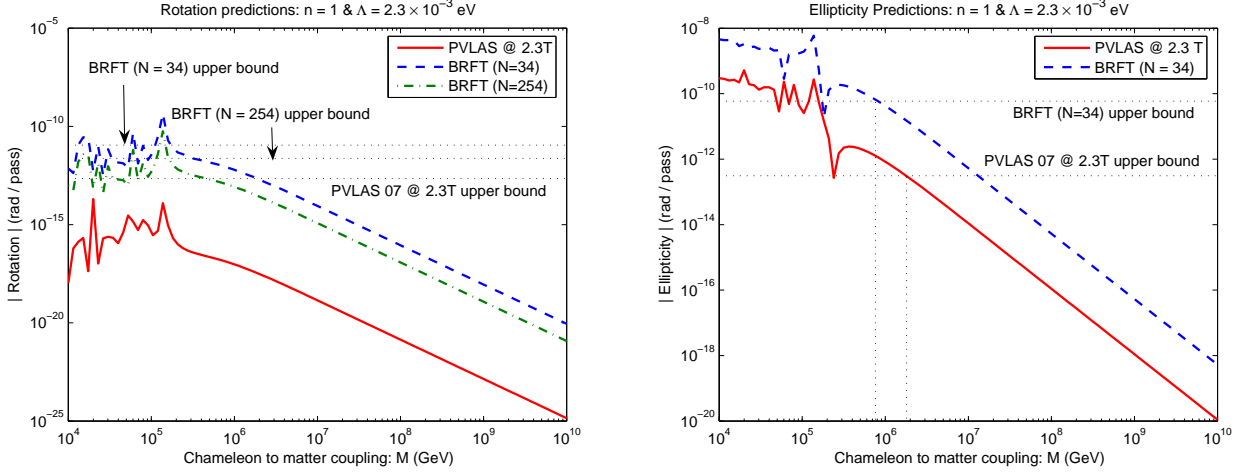


FIG. 5: Predictions for rotation (left) and ellipticity (right) in the chameleon model as a function of  $M$  for  $\Lambda = 2.3 \times 10^{-3}$  eV and  $n = 1$ . Predictions for the  $B = 2.3$  T PVLAS ( $L = 100$  cm,  $d = 270$  cm,  $\omega = 1.2$  eV,  $\rho_{\text{gas}} = 2 \times 10^{-14}$  gcm $^{-3}$  and  $\varphi = \pi/4$ ) and BRFT ( $B = 2$  T,  $L = 800$  cm,  $d = 345$  cm,  $\omega = 2.41$  eV,  $\rho_{\text{gas}} \approx 10^{-14}$  gcm $^{-3}$  and  $\varphi = \pi/4$ ) set-ups are shown. The thin-dotted lines show the 95% confidence upper bounds on both the rotation and the ellipticity.

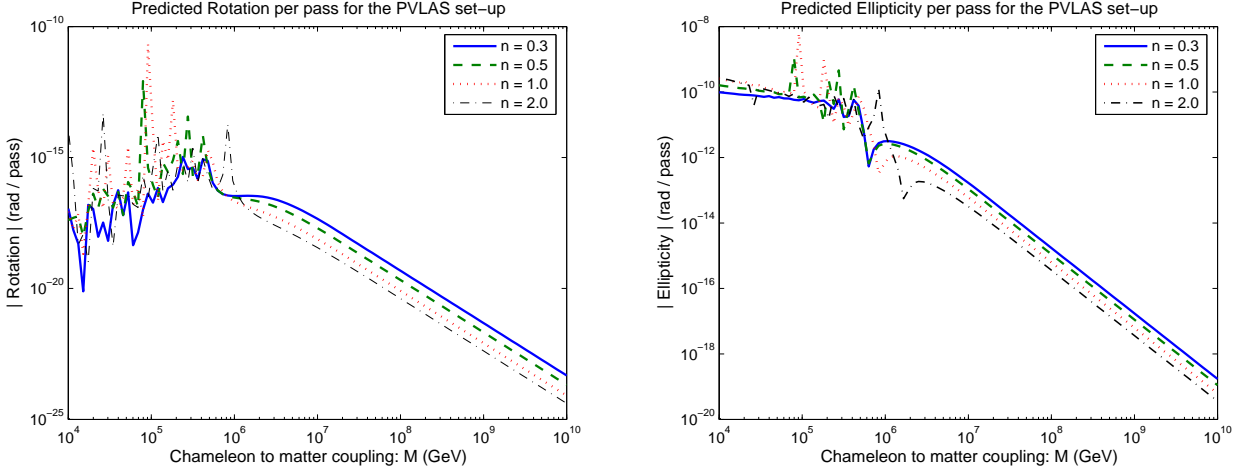


FIG. 6: Predictions for rotation (left) and ellipticity (right) in the chameleon model as a function of  $M$  for  $\Lambda = 2.3 \times 10^{-3}$  eV and different values of  $n$ . The PVLAS set-up is used ( $L = 100$  cm,  $d = 270$  cm,  $\omega = 1.2$  eV,  $B = 5$  T,  $\rho_{\text{gas}} = 2 \times 10^{-14}$  gcm $^{-3}$  and  $\varphi = \pi/4$ ).

$n$  and scale as  $B^2/M^2$ . Different  $\mathcal{O}(1)$  values of  $n$  do not, therefore, alter the magnitude or  $M$  dependence of either  $\psi$  or  $\Delta\varphi$  for  $M \gg 10^6$  GeV. If  $M \lesssim \mathcal{O}(10^6)$  GeV however, then  $X \gtrsim \mathcal{O}(1)$  then both  $\psi$  and  $\Delta\varphi$  depend strongly on  $m_\phi$  which in turn depends strongly on  $\rho_{\text{gas}}$ ,  $B$  and  $n$  for such values of  $M$ . We can clearly see this transition from strong to weak  $n$  dependence in Figure 6.

### C. Has a chameleon field already been detected?

The PVLAS 2007 results found no evidence for any ellipticity with  $B = 2.3$  T. However, at  $B = 5.5$  T a non-zero ellipticity was detected:  $\psi = (9.7 \pm 1.3) \times 10^{-8}$  with 45000 passes [10]. This is equivalent to an ellipticity per pass of:  $(2.2 \pm 0.3) \times 10^{-12}$ . If, as is the case for standard ALPs,  $\psi \propto B^2$  then such an ellipticity at 5.5 T implies that at 2.3 T, PVLAS should have found  $\psi = (1.7 \pm 0.2) \times 10^{-8}$  which is, in fact, ruled out with 99% confidence. A  $B^2$  scaling of  $\psi$  therefore implies that the signal detected with  $B = 5.5$  T must be of instrumental origin [10].

In chameleon theories, however,  $m_\phi^2$  can depend on  $B$  and so a  $B^2$  scaling of the ellipticity is not assured. We noted above that if  $X = m_\phi^2(2d + L)/2\omega \ll 1$  then both  $\psi$  and  $\Delta\phi$  scale as  $B^2$ . If we wish to reconcile the 5.5 T

detection with the 2.3 T null result we must therefore concentrate on  $\mathcal{O}(1)$  or greater values of  $X$ , which for PVLAS corresponds to  $m_\phi \gtrsim 3 \times 10^{-4} \text{ eV} \gg 2/R \approx 3 \times 10^{-5} \text{ eV}$ . We are therefore well into the region where  $m_\phi$  depends strongly on both  $\rho_{\text{gas}} + B^2/2$ . Now  $m_\phi$  grows with  $B^2$ , but it is generally the case that  $|\psi|$  decreases as  $m_\phi$  grows, and therefore  $\psi$  generally grows more slowly than  $B^2$  for  $X \sim \mathcal{O}(1)$ . However, we need a faster than  $B^2$  growth if we are to find a theory that predicts the signal seen at  $B = 5.5 \text{ T}$  without violating the  $B = 2.3 \text{ T}$  upper bound. Fortunately, the necessarily faster than  $B^2$  growth in  $|\psi|$  does occur in chameleon field theories when:

$$\frac{\Delta_r}{2} + \frac{m_\phi^2(B)2d + L}{4\omega} \approx m\pi,$$

for some integer  $m$ . Both  $\psi$  and  $\Delta\phi$  are strongly peaked about values of  $m_\phi$  that satisfy the above equation. In these cases all the effects that usually result in the chameleon and photon fields becoming decoherent cancel each other out, which results in a greatly amplified signal. For these values of  $m_\phi$  the experiment could be thought of as being resonant. The positions of these resonances are highly dependent on the set-up of the experiment. If  $m_\phi(B = 5.5 \text{ T})$  for  $B = 5.5 \text{ T}$  just so happens lies close to such a resonance but  $m_\phi(B = 2.3 \text{ T})$  does not, then we would have  $|\psi(B = 5.5 \text{ T})| \gg (5.5/2.3)^2 |\psi(B = 2.3 \text{ T})|$ . Additionally, since  $\psi$  changes sign as one passes through such a resonant point, we can ensure that  $\psi(B = 5.5 \text{ T}) > 0$ . In the context of standard ALPs,  $\psi > 0$  implies the existence of a pseudo-scalar, in the chameleon model, however, this is not the case and  $\psi$  can be both positive and negative depending on the value of  $m_\phi$ .

We find that for  $\Lambda = 2.3 \times 10^{-3} \text{ eV}$ , there exist values of  $M$  for which  $\psi(5.5 \text{ T}) = 9.7 \pm 1.3 \times 10^{-8}$  and  $|\psi(2.3 \text{ T})| < 1.4 \times 10^{-8}$  for  $n \gtrsim 2$ . In all cases  $M \sim \mathcal{O}(10^6 \text{ GeV})$  and  $m_\phi \sim \mathcal{O}(10^{-3} \text{ eV})$  with larger values of  $n$  corresponding to both larger values of  $M$  and smaller values of  $|\psi(2.3 \text{ T})|$ . For example: If  $n = 2$  then  $M = (1.13 \pm 0.03) \times 10^6 \text{ GeV}$  gives  $\psi(5.5 \text{ T}) = 9.7 \pm 1.3 \times 10^{-8}$ ,  $\psi(2.3 \text{ T}) = -(1.32 \pm 0.05) \times 10^{-8}$ ,  $\Delta\varphi(5.5 \text{ T}) = -(1.4 \pm 0.2) \times 10^{-12}$  and  $\Delta\varphi(2.3 \text{ T}) = -(1.6 \pm 0.1) \times 10^{-13}$ . If this is the case then the BMV experiment would measure  $\psi(BMV) \approx -7.3 \times 10^{-8}$ . If however  $n = 3$  then  $M = (1.58 \pm 0.04) \times 10^6 \text{ GeV}$  is required and  $|\psi(2.3 \text{ T})| < 4 \times 10^{-9}$ ; BMV would measure  $\psi(BMV) \approx -3.5 \times 10^{-7}$ . We have checked that these models would be not ruled out by the BRFT experiment. In all cases, the ellipticity and rotation predicted by these models in the context of that set-up is well below the BRFT upper bounds. This is due in part to the long length of the BRFT interaction region (8 m) which results in its sensitivity being peaked for particles with mass smaller than 1 meV. In contrast, all of the chameleon models that reproduce the signal observed by PVLAS have  $m > 1 \text{ meV}$  i.e. outside of the region where BRFT works best..

In the chameleon model then  $\psi(5.5 \text{ T}) = 9.7 \pm 1.3 \times 10^{-8}$  is not necessarily excluded by  $|\psi(2.3 \text{ T})| < 1.4 \times 10^{-8}$ , however it does require that chameleon mass for  $B = 5.5 \text{ T}$  lies very close to a resonant point. Since the position of these resonances is highly dependent on the set-up of the experiment this would be a remarkable coincidence. This issue will certainly be settled by the upcoming BMV experiment.

## VI. DISCUSSION AND CONCLUSIONS

In this paper we have studied how chameleon fields that couple to the electromagnetic sector alter the propagation of photons in a vacuum. Just as other axion like particles (ALPs) do, such chameleon fields would induce both dichroism (rotation) and birefringence (ellipticity) in a photon beam travelling through a magnetic field. Both of these effects could be detected by laboratory searches for ALPs such as PVLAS [6], Q&A [24] and BMV [29, 30]. The mass of a chameleon field depends on its environment; specifically it is larger in backgrounds where the ambient matter density is high than it is in those where the background density is low. The mass and coupling strength of standard (i.e. non-chameleonic) ALPs are strongly constrained by limits on solar axion production. As was pointed out in [5], however, the density dependence of the chameleon's mass implies that  $m_\phi$  in the Sun is generally much larger than the value of  $m_\phi$  in the laboratory vacuum. Solar axion production therefore represents a far less stringent constraint on chameleon ALPs than it does on standard ALPs. This opens to the door to the prospect that chameleons fields, if they exist, may well be detected first by ongoing and upcoming laboratory axion searches.

The original motivation for this work was the reported detection of light polarization rotation in the vacuum in the presence of a magnetic field by the PVLAS experiment [6]. If one wishes to explain this detection by the presence of a standard ALPs then it must have mass  $m_{ALP} \approx 1 \text{ meV}$  and photon coupling  $M \approx 10^6 \text{ GeV}$ . A standard ALP with these properties is, however, strongly ruled out by bounds on solar axion production [5], and if the ALP is a scalar field then it is additionally ruled out by short-range laboratory tests of gravity. However, as was shown in [5], a chameleon field with these properties is *not* ruled out. If chameleon fields behaved the same as standard ALPs they could, at first sight, explain the PVLAS detection.

In this paper we have shown that, within the confines of experiments like PVLAS, chameleon fields and standard ALPs behave very differently. As a photon beam moves through the experiment it generates ALPs. In the absence of a chameleon mechanism these ALPs pass through the mirrors at either end of the Fabry-Perot cavity and escape

the experiment. Chameleon fields, however, do not escape. As a direct result of their chameleonic properties, the chameleon mass  $m_\phi$  in the mirrors is many orders of magnitude larger than  $m_\phi$  in the cavity. The mirrors therefore act as a potential well for the chameleon particles and, as was shown above, these particles do not have energy to propagate through the mirrors. Not only then do the photons reflect off the mirrors, but so also do the chameleon particles. Furthermore, whereas the photons reflect off the surface of the mirror, a beam of chameleon particles with energy  $\omega$  was found to reflect at a distance  $\mathcal{O}(1/\omega)$  away from the surface of the mirror. A coherent beam of photons and chameleons incident on the mirror is therefore decoherent after reflection. The presence of these two effects means that the standard expressions for the rotation and ellipticity no longer hold. In Section IV we therefore derived new expressions for the dichroism and birefringence induced in a photon beam by the presence of a chameleon field. The new expressions for the rotation and ellipticity are given respectively by Eqs. (52) and (53).

The combination of both the reflection and decoherence of the chameleon particles was seen to lead to the magnitude of the predicted ellipticity always being much larger than that of the predicted rotation. Specifically, if the photon beam makes  $N$  passes through the Fabry-Perot cavity, then the ratio of the rotation to the ellipticity is  $\mathcal{O}(1/N) \ll 1$ . The large ellipticity to rotation ratio is a generic feature of chameleon theories, and so experimental searches for birefringence are better placed to detect / rule out the existence of chameleon particles than measurements of rotation.

In Section V we used our expressions for the rotation and ellipticity to make predictions for the PVLAS [6], Q&A [24] and upcoming BMV [29, 30] experiments. The magnitude of the potentially detectable signal was found to depend heavily on the density of the laboratory vacuum. The relatively high density vacuum used in the Q&A experiment was seen to result in a much smaller predicted rotation and ellipticity than that for the PVLAS and BMV set-ups. If we assume that the non-zero ellipticity detected by PVLAS with  $B = 5.5$  T is instrumental then the most recent PVLAS results constrain  $M \gtrsim 2 \times 10^6$  GeV for  $n = 1$  and  $\Lambda = 2.3 \times 10^{-3}$  eV, with a similar bound for other  $\mathcal{O}(1)$  values of  $n$ . BMV will be able to detect or rule out the presence of chameleon fields with  $\Lambda = 2.3 \times 10^{-3}$  eV and  $M \lesssim 3 \times 10^7$  GeV. On the other hand, if the  $B = 5.5$  T ellipticity signal is physical, then chameleon theories can provide an explanation with a mass  $m_\phi \approx 10^{-3}$  eV and an inverse coupling  $M \approx 10^6$  GeV. In this case, a large ellipticity should be observed by the BMV experiment, providing a decisive tests of chameleon theories.

In conclusion, chameleon theories can be tested with light propagating in vacuum through a magnetic field as long as the coupling to the electromagnetic sector is large enough ( $M \ll M_{\text{Pl}}$ ). Chameleon theories are then an additional interesting class of models to be probed by experiments of PVLAS-type. We found that the predictions of chameleon theories are substantially different from those of standard ALPs and as such could potentially reconcile astrophysical with local tests. These experiments provide additional constraints on the parameter of the theory, which are complementary to gravitational and/or Casimir-experiments.

## APPENDIX A: GENERALIZED CALCULATION OF PROPAGATION OF LIGHT AND THE CHAMELEON IN A CAVITY

In Section IV we calculated how light and the chameleon field propagate in a cavity under the assumptions there is no gap between the mirrors and the ends of the interaction region and if the photon and chameleon field reflect in the same manner. In general neither of these two assumptions hold. The calculation performed in Section IV is very direct and elegant however we found that it becomes significantly more complicated when the assumptions are dropped. In the limit where both of the aforementioned assumptions hold, the results found using this alternative approach are entirely equivalent to those found in Section IV. In this appendix our method is based on that used in [20].

Waves in the photon field,  $\mathbf{A}$ , and in the chameleon field,  $\phi$ , obey:

$$\square \mathbf{A} = \frac{\nabla \phi \times \mathbf{B}}{M}, \quad (\text{A1})$$

$$\square \phi - m_\phi^2 \phi = \frac{\mathbf{B} \cdot (\nabla \times \mathbf{A})}{M}. \quad (\text{A2})$$

We take  $\mathbf{B} = B\mathbf{e}_x$ ,  $\mathbf{A} = a_{\parallel}\mathbf{e}_x + a_{\perp}\mathbf{e}_y$ . The waves then travel in the  $z$ -direction. We take the interaction region, where  $B \neq 0$ , to have length  $L$ . There is a distance  $d$  between the ends of the interaction region and the mirrors.

For right moving waves  $\propto \exp(ikz)$ , in the interaction region, we have:

$$\partial_t^2 a_{\parallel} = -k^2 a_{\parallel},$$

and

$$-\partial_t^2 \mathbf{v} = U_r \mathbf{v}, \quad (\text{A3})$$



where

$$\mathbf{v} = \begin{pmatrix} a_{\perp} \\ \chi \end{pmatrix},$$

$$U_r = \begin{pmatrix} k^2 & -kB/M \\ -kB/M & k^2 + m^2 \end{pmatrix},$$

and where  $\chi = i\phi$ . The eigenvectors of  $U_r$  are:

$$\begin{pmatrix} \cos \theta \\ \sin \theta \end{pmatrix}, \quad \begin{pmatrix} -\sin \theta \\ \cos \theta \end{pmatrix},$$

with eigenvalues  $\omega_{-}^2$  and  $\omega_{+}^2$  respectively where:

$$\omega_{\pm}^2 = k^2 + m^2 \frac{\cos 2\theta \pm 1}{2 \cos 2\theta}. \quad (\text{A4})$$

As in Section IV we have defined:

$$\tan 2\theta = \frac{2Bk}{Mm^2}.$$

Eq. (A3) can then be written as:

$$-\partial_t^2 \mathbf{v} = Q_+^T \Omega Q_+ \mathbf{v},$$

where

$$Q_+ = \begin{pmatrix} \cos \theta & -\sin \theta \\ \sin \theta & \cos \theta \end{pmatrix},$$

and  $\Omega = \text{diag}(\omega_{-}^2, \omega_{+}^2)$ . A similar equation holds for the left-moving modes:

$$-\partial_t^2 \mathbf{v} = Q_-^T \Omega Q_- \mathbf{v},$$

where

$$Q_- = \begin{pmatrix} -\cos \theta & \sin \theta \\ \sin \theta & \cos \theta \end{pmatrix}.$$

In the interaction region then the evolution of the right moving modes is given by:

$$\mathbf{v}(t) = e^{-i\omega t} V_+(t) \mathbf{v}(0),$$

and the evolution of the left moving modes by:

$$\mathbf{v}(t) = e^{-i\omega t} V_-(t) \mathbf{v}(0),$$

where  $V_{\pm} = Q_{\pm}^T \text{diag}(e^{-i(\omega_{-}-\omega)t}, e^{-i(\omega_{+}-\omega)t}) Q_{\pm}$ . For  $t = L$  we have:

$$V_{\pm}(L) = \begin{pmatrix} c_{\pm} & \pm b \\ \pm b & c_{\pm} \end{pmatrix}, \quad (\text{A5})$$

where:

$$c_{\pm} = \cos^2 \theta e^{-i(\omega_{\mp}-\omega)L} + \sin^2 \theta e^{-i(\omega_{\pm}-\omega)L}, \quad (\text{A6})$$

$$b = \left( e^{-i(\omega_{-}-\omega)L} - e^{-i(\omega_{+}-\omega)L} \right) \frac{\sin 2\theta}{2}. \quad (\text{A7})$$

Thus a wave that enters the magnetic field region at  $z = 0$  as  $\mathbf{v}_0$  will, upon exiting, the field region at  $z = L$  have evolved into:

$$\mathbf{v}(L) = e^{-i\omega L} V_+(L) \mathbf{v}_0.$$

The wave then exits the magnetic field, travels a distance  $d$  to the mirror, is reflected, travels a further distance  $d$  and re-enters the magnetic field at  $z = L$ . Outside the interaction region the chameleon field travels more slowly than the photon, and furthermore it may reflect at a different point. In general then the chameleon will return to  $z = L$  having been shifted by a phase relative to the photon field. We define this phase to be  $\Delta$ . The assumption made in Section IV are equivalent to taking  $\Delta = 0$ . We calculate this  $\Delta$  in Appendix B.

When the fields re-enters the field region, this time moving leftwards, they are therefore (up to an overall irrelevant phase factor) in a state:

$$\mathbf{v} = e^{-i\omega L} R V_+(L) \mathbf{v}_0,$$

where  $R = \text{diag}(1, -\exp(-i\Delta))$ . The  $-$  sign is in the last component of  $R$  due to the fact that chameleons are scalar fields with positive parity, whereas the photon fields are vectors with negative parity. The fields then travels through the interaction region, this time moving leftwards, exit the region and reflect back again, so that by the time they have returned to  $z = 0$  moving rightwards they are in a state:

$$\mathbf{v}_{\text{round}} = e^{-2i\omega L} (R V_- R V_+) \mathbf{v}_0.$$

If  $\Delta$  is taken to have an imaginary part then this analysis also allows us to account for any scalar fields that escape the cavity. For instance if, as is often taken to be case when the ALP is not a chameleon, the scalar field does *not* reflect then  $\Delta = -i\infty$ , and  $R = \text{diag}(1, 0)$ . We define:

$$F = R V_- R V_+ = \begin{pmatrix} \alpha & \gamma \\ e^{-i\Delta} \gamma & e^{-i\Delta} \beta \end{pmatrix}, \quad (\text{A8})$$

where

$$\alpha = c_+^2 + e^{-i\Delta} b^2, \quad \beta = c_-^2 e^{-i\Delta} + b^2, \quad \gamma = b(c_+ + e^{-i\Delta} c_-).$$

Then after  $N$  passes through the interaction region, the fields will be in a state:

$$\mathbf{v}_N = e^{-2i\omega N L} F^N \mathbf{v}_0.$$

We define

$$F^N \mathbf{v}_0 = \begin{pmatrix} A_N \\ Z_N \end{pmatrix},$$

and find that:

$$A_{N+1} = \alpha A_N + \gamma Z_N, \quad (\text{A9})$$

$$Z_{N+1} = e^{-i\Delta} \gamma A_N + e^{-i\Delta} \beta Z_N, \quad (\text{A10})$$

and so:

$$A_{N+1} = (\alpha + \beta e^{-i\Delta}) A_N + e^{-i\Delta} [\gamma^2 - \alpha\beta] A_{N-1}. \quad (\text{A11})$$

We take initial conditions  $A_0 = \sin \varphi$  and  $Z_0 = 0$  which implies that  $A_1 = \alpha \sin \varphi$ . We then find the solution:

$$\frac{A_N}{\sin \varphi} = \left( \frac{\alpha - \mu_-}{\mu_+ - \mu_-} \mu_+^N - \frac{\alpha - \mu_+}{\mu_+ - \mu_-} \mu_-^N \right), \quad (\text{A12})$$

where

$$\mu_+ = \alpha + e^{-i\Delta} \delta\mu, \quad (\text{A13})$$

$$\mu_- = e^{-i\Delta} (\beta - \delta\mu), \quad (\text{A14})$$

where

$$e^{-i\Delta} \delta\mu = \frac{\alpha - \beta e^{-i\Delta}}{2} \left( (1 + e^{-i\Delta} \nu^2)^{1/2} - 1 \right),$$

and

$$\nu = \frac{2\gamma}{(\alpha - \beta e^{-i\Delta})} = \frac{2b}{c_+ - e^{-i\Delta}c_-}.$$

If  $\Delta = 0$  then:

$$\mu_{\pm} = e^{-i(\omega_{\mp} - \omega)L}.$$

We take  $\theta \ll 1$  and so:

$$e^{-i\Delta}\delta\mu \approx \frac{\gamma^2 e^{-i\Delta}}{\alpha - \beta e^{-i\Delta}} = \frac{e^{-i\Delta}b^2(c_+ + e^{-i\Delta}c_-)}{c_+ - c_- e^{-i\Delta}} \propto \theta^2 \ll 1.$$

We define  $\delta_{\pm}/2\omega = \omega_{\pm} - \omega$  and  $\delta = \delta_+ - \delta_-$ . For small  $\theta$ ,  $\delta_- = \mathcal{O}(\theta^2)$ .

After  $N$  round trips, a photon which was initial in a state  $(\cos\varphi, \sin\varphi)^T$  has evolved into:

$$\begin{pmatrix} a_{\parallel}(N) \\ a_{\perp}(N) \end{pmatrix} = \begin{pmatrix} \eta(N) \cos(\varphi + \Delta\varphi(N)) \\ \eta(N) \sin(\varphi + \Delta\varphi(N)) e^{i\rho(N)} \end{pmatrix} = \begin{pmatrix} \cos\theta \\ \frac{\tan(\varphi + \Delta\varphi(N))}{\tan\varphi} e^{i\rho(N)} \sin\theta \end{pmatrix},$$

where

$$\frac{\tan(\varphi + \Delta\varphi(N)) e^{i\rho(N)}}{\tan\varphi} = \frac{A_N}{\sin\theta}. \quad (\text{A15})$$

Since the photon is trapped in the cavity, what one actually measures is a superposition of states which have each completed a different number of passes. One therefore measures:

$$\mathbf{a}_{\text{measured}} = \frac{1}{N+1} \sum_{k=0}^N \mathbf{a}(k) = \begin{pmatrix} \cos\theta \\ \frac{\tan(\varphi + \Delta\varphi_m)}{\tan\varphi} e^{i\rho_m} \sin\theta \end{pmatrix},$$

where

$$\frac{\tan(\varphi + \Delta\varphi_m) e^{i\rho_m}}{\tan\varphi} = \frac{1}{N+1} \sum_{k=0}^N \frac{A_k}{\sin\theta}.$$

We calculate  $\Delta\phi_m$  and  $\rho_m$  to  $\mathcal{O}(\theta^2)$ . To this order

$$\mu_- \approx e^{-2i\Delta} e^{-i\delta_+ L/\omega} \left( 1 + 2\theta^2 \left[ \frac{(1 - e^{-i\Delta})(1 - e^{-i\delta L/2\omega})}{1 - e^{-i\Delta - i\delta L/2\omega}} \right] \right), \quad (\text{A16})$$

$$\mu_+ = e^{-i\delta_- L/\omega} \left( 1 - 2\theta^2 \left[ \frac{(1 - e^{-i\Delta})(1 - e^{-i\delta L/2\omega})}{1 - e^{-i\Delta - i\delta L/2\omega}} \right] \right). \quad (\text{A17})$$

We define

$$H_{\Delta}(x) = \left( \frac{\sin(x/2)}{\sin(\Delta/2 + x/2)} \right)^2.$$

Assuming that  $\theta^2 H_{\Delta}(\delta L/2\omega) \ll 1$ , we perform the sum over the  $A_k$  and find that we find:

$$\begin{aligned} \frac{\tan(\varphi + \Delta\varphi_m) e^{i\rho_m}}{\tan\varphi} = & 1 - \theta^2 H_{\Delta} \left( \frac{\delta L}{2\omega} \right) - iN \left[ \frac{\delta_- L}{2\omega} + \theta^2 G_{\Delta} \left( \frac{\delta L}{2\omega} \right) \right] \\ & + \theta^2 e^{-iN\Delta - \frac{iN\delta L}{2\omega}} H_{\Delta} \left( \frac{\delta L}{2\omega} \right) \delta_N \left( \Delta + \frac{\delta L}{2\omega} \right), \end{aligned} \quad (\text{A18})$$

where we have defined

$$G_{\Delta}(x) = \frac{2 \sin(\Delta/2) \sin(x/2)}{\sin(\Delta/2 + x/2)},$$

and

$$\delta_N(x) = \frac{\sin((N+1)x)}{(N+1)\sin x}.$$

If  $\Delta = 0$  then  $G_\Delta = 0$  and  $H_\Delta = 1$ . The rotation is given by  $\Delta\phi_m$  and the ellipticity by  $\psi = -\rho_m \sin 2\varphi/2$ . For general real  $\Delta$  we therefore find:

$$\begin{aligned} \frac{\Delta\varphi}{\sin 2\varphi} = & - \left( \frac{B\omega}{Mm_\phi^2} \right)^2 H_\Delta \left( \frac{m_\phi^2 L}{2\omega} \right) \left\{ \frac{1}{2} + \left[ \sin^2 \left( \frac{N\Delta}{2} + \frac{Nm_\phi^2 L}{4\omega} \right) \right. \right. \\ & \left. \left. - \frac{1}{2} \right] \delta_N \left( \Delta + \frac{m_\phi^2 L}{2\omega} \right) \right\}, \end{aligned}$$

and the ellipticity is

$$\begin{aligned} \frac{\psi}{\sin 2\varphi} = & - \frac{1}{2} \left( \frac{B\omega}{Mm_\phi^2} \right)^2 \left\{ \frac{Nm_\phi^2 L}{2\omega} - NG_\Delta \left( \frac{m_\phi^2 L}{2\omega} \right) \right. \\ & \left. - \sin \left( N\Delta + \frac{Nm_\phi^2 L}{2\omega} \right) H_\Delta \left( \frac{m_\phi^2 L}{2\omega} \right) \delta_N \left( \Delta + \frac{m_\phi^2 L}{2\omega} \right) \right\}. \end{aligned}$$

As a consistency check we can also consider the case where the scalar fields escape after every pass. This is given by taking  $\exp(-i\Delta) \rightarrow 0$ , and in this limit  $H_\Delta \rightarrow 0$  and  $G_\Delta(x) \rightarrow \sin(x)2i \sin^2(x/2)$  and so we recover the standard formulae:

$$\frac{\Delta\varphi_{escape}}{\sin 2\varphi} = - \left( \frac{B\omega}{Mm_\phi^2} \right)^2 \sin^2 \left( \frac{m_\phi^2 L}{4\omega} \right),$$

and

$$\frac{\psi_{escape}}{\sin 2\varphi} = - \frac{1}{2} \left( \frac{B\omega}{Mm_\phi^2} \right)^2 \left[ \frac{Nm_\phi^2 L}{2\omega} - N \sin \left( \frac{m_\phi^2 L}{2\omega} \right) \right].$$

In Appendix B we consider the propagation and reflection of the chameleon field outside the interaction region and evaluate  $\Delta$ .

## APPENDIX B: REFLECTION OF THE CHAMELEON FIELD

We consider how chameleon waves with frequency  $\omega$  reflect off a flat mirror that is placed at  $z = z_0$ , and propagate relative to a photon field outside the interaction region. We write  $\phi = \phi_0(z) + \delta\phi(z, t)$ , where  $\delta\phi$  is a small perturbation with frequency  $\omega$ , and  $\phi_0$  is the background value of  $\phi$ . We begin by showing that  $m_\phi \sim 1/(z - z_0)$  near the mirror.

### 1. Behaviour of the chameleon mass near a mirror

We define  $\rho_m$  to be the density of the mirror and define  $\phi_m$  by:

$$V'(\phi_m) = -\frac{\rho_m}{M}.$$

We define  $m_m = m_\phi(\phi_m)$ . We take the mirror to lie in the region  $z < z_0$  with its surface at  $z = z_0$ . Since  $M \ll M_{Pl}$ ,  $\phi_0$  must be  $\approx \phi_m$  deep inside the mirror for consistency with experimental tests of gravity. Inside the mirror,  $\phi_0$  obeys

$$\frac{d^2\phi_0}{dz^2} = V'(\phi_0) + \frac{\rho_m}{M},$$

and outside the mirror ( $z > z_0$ ), where the density of matter is  $\rho_{\text{gas}}$ , we have

$$\frac{d^2\phi_0}{dz^2} = V'(\phi_0) + \frac{\rho_{\text{gas}}}{M}.$$

We define  $\phi_c$  by:

$$V'(\phi_c) = -\frac{\rho_{\text{gas}}}{M},$$

and  $m_c = m_\phi(\phi_c)$ . Integrating the above equations and assuming that deep inside the mirror  $\phi \rightarrow \phi_m$  and  $d\phi/dz \rightarrow 0$  we find:

$$\frac{1}{2} \left( \frac{d\phi_0}{dz} \right)^2 = V(\phi_0(z)) - V(\phi_m) + \frac{\rho_m}{M}(\phi_0(z) - \phi_m) \quad z < z_0, \quad (\text{B1})$$

$$\frac{1}{2} \left( \frac{d\phi_0}{dz} \right)^2 = V(\phi_0(z)) - V(\phi_c) + \frac{\rho_{\text{gas}}}{M}(\phi_0(z) - \phi_c) \quad z > z_0. \quad (\text{B2})$$

Matching these equations at  $z = z_0$  and using  $\rho_m \gg \rho_{\text{gas}}$  we find that at  $z = z_0$ :

$$\phi_0(z = z_0) \approx \phi_m - \frac{V(\phi_m) - V(\phi_c)}{V'(\phi_m)}. \quad (\text{B3})$$

From Eq. (B2), we see that outside the mirror, in the region where  $|V'(\phi_c)/V'(\phi_0)| \ll 1$ , we have:

$$\frac{1}{2} \left( \frac{d\phi_0}{dz} \right)^2 = V(\phi_0) - V(\phi_c).$$

We now normalize the potential  $V$  so that as  $\rho_{\text{gas}} \rightarrow 0$ ,  $V(\phi_c(\rho_{\text{gas}})) \rightarrow 0$ , i.e. we neglect any constant term in  $V$ .  $|V'(\phi_c)/V'(\phi_0)| \ll 1$  then implies than  $V(\phi_0) \gg V(\phi_c)$  and so:

$$a_\phi \frac{d(1/m_0)}{dz} = 1, \quad (\text{B4})$$

where

$$a_\phi = \frac{\sqrt{2}(V''(\phi_0))^{3/2}}{(-V'''(\phi_0))(V(\phi_0))^{1/2}} > 0.$$

If  $V \propto \phi^{-n}$  then  $a_\phi = \sqrt{2n(n+1)/(n+2)^2}$ . We define  $a_\phi(z_0) = a_s$  and use the shorthand  $a_\phi(\phi(z)) = a_\phi(z)$ , we then have:

$$\frac{1}{m_0} = \frac{1}{m_s} + \frac{z - z_0}{a_\phi(z)} + \frac{1}{a_\phi(z)} \int_{a_s}^{a_\phi(z)} \frac{1}{m_0} da_\phi. \quad (\text{B5})$$

In many theories, the potential is such that  $a_\phi$  changes only very slowly i.e.  $|d \ln a_\phi/dx| \ll |d \ln m_0/dx|$  for  $\omega \lesssim m_0 \lesssim m_m$ ; when this is true we have:

$$m_0 \approx \frac{a_\phi(z)}{z - z_0 + a_\phi(z)/m_s}, \quad (\text{B6})$$

where  $a_\phi(z)$  is slowly varying compared to  $m_0$  and  $m_s \equiv \sqrt{V''(\phi_0(z = z_0))}$  is the mass of the chameleon on the surface of the mirror.

Since we have assumed that  $|V'(\phi_c)/V'(\phi_0)| \ll 1$  then we must have  $m_0(z) \gg m_c$  which implies  $z - z_0 \ll 1/m_c$ . For  $1/m_m \lesssim 1/m_s \ll \Delta z = z - z_0 \ll 1/m_c$ , Eq. (B6) gives  $m_0 \propto 1/\Delta z$ .

This behaviour will occur in any chameleon theory where  $a_\phi$  varies slowly with  $\phi$  compared to  $m_\phi$ . More generally, we have:

$$m_0 \geq \frac{a_\phi(z)}{z - z_0 + a_\phi(z)/m_s},$$

if

$$b_\phi(\phi) \equiv \frac{2V''''V''}{3V''''^2} + \frac{V''V'}{3V''''V} \leq 1,$$

and  $m_0 \leq a_\phi/(z - z_0 + a_\phi/m_s)$  if  $b_\phi \geq 1$ . The assumption that  $a_\phi$  is slowly varying compared to  $1/m_0$  is equivalent to  $3|1 - b_\phi| \ll 1$  for  $m_0 < m_\phi < m_s \lesssim m_m$ .

## 2. Reflection of chameleon waves

We now consider the reflections of chameleon waves:  $\delta\phi = \delta\tilde{\phi}(z)e^{-i\omega t}$ . These evolve according to:

$$\frac{d^2\delta\tilde{\phi}}{dz^2} \approx (V''(\phi_0) - \omega^2) \delta\tilde{\phi}.$$

For most sensible choices of potential we have  $m_s \sim O(m_m = m_\phi(\phi_m))$  and we assume that  $m_m \gg \omega$ ; which must certainly be the case if  $\omega \sim \mathcal{O}(1)$  eV and the constraints on solar axion production are satisfied [5]. For  $z \lesssim z_0$  then we have  $\delta\tilde{\phi} \approx C \exp(m_{eff}(z)(z - z_0))$  where  $m_{eff}(z) \sim O(m_\phi(\phi_m))$  and  $C$  is a constant.

The behaviour of  $m_0$  for  $m_0 \gg m_c \equiv m_\phi(\phi_c)$  is given by Eq. (B6). In the experiments that we consider  $m_c \ll \omega$ . The behaviour of  $m_0$  for  $m_0 \ll \omega$  only effects this reflection calculation at sub-leading order and so, to a first approximation we have taken  $m_0(z)$  to be given by Eq. (B6). Defining  $x = z - z_0 + a_\phi/m_s$ , we find that near the mirror we have:

$$\frac{d^2\delta\tilde{\phi}}{dx^2} \approx \left( \frac{a_\phi^2}{x^2} - \omega^2 \right) \delta\tilde{\phi},$$

which has solutions:

$$\delta\tilde{\phi} = \sqrt{\omega x} (c_1 J_\alpha(\omega x) + c_2 N_\alpha(\omega x)),$$

where  $J_\alpha$  and  $N_\alpha$  are Bessel functions and  $\alpha = \frac{1}{2}\sqrt{1 + 4a_\phi^2}$ . Near  $z = z_0$  we have  $\omega x \approx a_\phi\omega/m_s \equiv \delta$ . Generally  $\delta = a_\phi\omega/m_s \sim O(\omega/m_m) \ll 1$ . Matching at  $z = z_0$  we find:

$$C = \sqrt{\delta}(c_1 J_\alpha(\delta) + c_2 N_\alpha(\delta)), \quad (\text{B7})$$

$$m_1 \delta C = \frac{1}{2}\sqrt{\delta}(c_1 (J_\alpha(\delta) + 2\delta J'_\alpha(\delta)) + c_2 (N_\alpha(\delta) + 2\delta N'_\alpha(\delta))), \quad (\text{B8})$$

where  $m_1 \sim O(m_s)$  is given by  $m_1 = d \exp(-m_{eff}(z)(z - z_0))/dz|_{z=z_0}$ . The precise value of  $m_1$  is generally not important. We find then that:

$$c_2 = B(\delta)c_1,$$

where

$$B(\delta) = \left( \frac{m_1 \delta - \frac{1}{2} + \frac{\delta J'_\alpha(\delta)}{J_\alpha(\delta)}}{m_1 \delta - \frac{1}{2} + \frac{\delta Y'_\alpha(\delta)}{Y_\alpha(\delta)}} \right) \frac{J_\alpha(\delta)}{Y_\alpha(\delta)}.$$

In general  $\delta \ll 1$  which implies that  $B(\delta) \ll 1$  and so  $c_2 \ll c_1$ . A distance  $z \gg 1/m_\phi(\phi_c)$  from the mirror then  $\delta\phi$  is therefore given by:

$$\delta\tilde{\phi} \approx \sqrt{\frac{2}{\pi}} c_1 \sin \left( \omega(z - z_0) - \left( \frac{\pi\alpha}{2} - \frac{\pi}{4} \right) \right). \quad (\text{B9})$$

We write:

$$\delta\phi = \phi_0 e^{-i\omega t} \left( e^{-ik(z-d-z_0)} - e^{ik(z-d-z_0)-i\Delta_r+i\omega 2d} \right).$$

A chameleon wave that leaves the interaction region, reflects off the mirror is therefore, on its return to the interaction region, shifted by a phase  $\Delta \equiv 2(k - \omega)d + \Delta_r$  relative to a photon that has made the same journey. From Eq. (B9) we have

$$\Delta_r = \frac{\pi}{2}(2\alpha - 1) = \frac{\pi}{2} \left( \sqrt{1 + 4a_\phi^2} - 1 \right). \quad (\text{B10})$$

If  $\Delta_r \ll 1$  then the additional phase-shift due to the the chameleon travelling more slowly than the speed of light (the  $2(k - \omega)d$  term in  $\Delta$ ) might be important. Taking  $k = \sqrt{\omega^2 - m_\phi^2(\phi_m)}$ , we find:

$$\Delta_m = 2(\omega - k)d \approx \frac{m_c^2 d}{\omega}.$$

We therefore we find:

$$\Delta = \Delta_r + \Delta_m \approx \frac{\pi}{2} \left( \sqrt{1 + 4a_\phi^2} - 1 \right) + \frac{m_c^2 d}{\omega}.$$

Throughout this work we have been primarily concerned with inverse power law potentials:  $V - \Lambda^4 \propto \phi^{-n}$  for  $n > 0$ . Valid chameleon theories exist with  $n = -2m$ , where  $m$  is a positive integer. In a more general scenario the potential might, around the point where  $m_\phi \approx \omega$  look locally like  $c_0 + c_1 \phi^{-n}$ , for some  $c_0$  and  $c_1$ , or any  $n$ . For such theories if  $n < -2$  or  $n > -2/3$  then we have:

$$\Delta_r = \frac{\pi n}{n + 2},$$

whereas if  $-2 < n < -2/3$  we find:

$$\Delta_r = -\frac{\pi(n + 1)}{2(n + 2)}.$$

### ACKNOWLEDGEMENTS

We are grateful to G. Cantatore, H. Gies, H. Mei, A. Ringwald and C. Rizzo for sharing information about the experiments and useful comments on a draft of this paper. CvdB and ACD are supported partly by PPARC DFM is supported by the Alexander von Humboldt Foundation. DJS is supported by PPARC.

### REFERENCES

- 
- [1] J. Khoury and A. Weltman, Phys. Rev. Lett. **93**, 171104 (2004); Phys. Rev. D **69**, 044026 (2004).  
[2] D. F. Mota and D. J. Shaw, Phys. Rev. D. **75**, 063501 (2007); Phys. Rev. Lett. **97** (2006) 151102.  
[3] Ph. Brax, C. van de Bruck, A.-C. Davis, J. Khoury and A. Weltman, Phys. Rev. D **70**, 123518 (2004).  
[4] Ph. Brax, C. van de Bruck, A. C. Davis and A. M. Green, Phys. Lett. B **633**, 441 (2006).  
[5] Ph. Brax, C. van de Bruck, A. C. Davis, [arXiv:hep-ph/0703243](#)  
[6] E. Zavattini *et al.* [PVLAS Coll.], Phys. Rev. Lett. **96**, 110406 (2006).  
[7] A. Ringwald, J. Phys. Conf. Ser. **39** (2006) 197  
[8] J. Jaeckel, E. Masso, J. Redondo, A. Ringwald and F. Takahashi, Phys. Rev. D **75** (2007) 013004  
[9] C. Robilliard, R. Battesti, M. Fouche, J. Mauchain, A. M. Sautivet, F. Amiranoff and C. Rizzo, [arXiv:0707.1296](#) [hep-ex].  
[10] E. Zavattini *et al.*, [arXiv:0706.3419](#) [hep-ph]  
[11] E. Masso and J. Redondo, JCAP **0509** (2005) 015 [[arXiv:hep-ph/0504202](#)].  
[12] P. Jain and S. Mandal, Int. J. Mod. Phys. D **15** (2006) 2095 [[arXiv:astro-ph/0512155](#)].  
[13] E. Masso and J. Redondo, Phys. Rev. Lett. **97** (2006) 151802 [[arXiv:hep-ph/0606163](#)].  
[14] R. N. Mohapatra and S. Nasri, Phys. Rev. Lett. **98** (2007) 050402 [[arXiv:hep-ph/0610068](#)].  
[15] S. A. Abel, J. Jaeckel, V. V. Khoze and A. Ringwald, [arXiv:hep-ph/0608248](#).  
[16] H. Gies, J. Jaeckel and A. Ringwald, Phys. Rev. Lett. **97**, 140402 (2006)  
[17] M. Ahlers, H. Gies, J. Jaeckel and A. Ringwald, Phys. Rev. D **75** (2007) 035011  
[18] X. P. Hu and Y. Liao, [arXiv:hep-ph/0702111](#).  
[19] S. I. Kruglov, Phys. Rev. D **75** (2007) 117301.  
[20] Y. Liao, [arXiv:0704.1961](#) [hep-ph], to appear in Phys.Lett.B  
[21] R. Battesti *et al.*, [arXiv:0705.0615](#) [hep-ex].  
[22] M. Ahlers, H. Gies, J. Jaeckel, J. Redondo and A. Ringwald, [arXiv:0706.2836](#) [hep-ph].  
[23] R. Cameron *et al.* [BRFT Coll.], Phys. Rev. D **47**, 3707 (1993)  
[24] W. T. Ni in *Frontier Tests of QED and Physics of the Vacuum*, edited by E. Zavattini *et al.* (Sofia: Heron Press, 1998), pp. 83 and references therein; S. J. Chen *et al.*, [arXiv:hep-ex/0308071](#) and references therein.  
[25] A. Ringwald, [arXiv:0704.3195](#) [hep-ph].  
[26] L. Maiani, R. Petronzio and E. Zavattini, Phys. Lett. B **175**, 359 (1986)  
[27] Bardeen, W.A., Gastmans, R and Lautrup, B., Nucl.Phys.B. **46**, 319 (1972); Carlson, E.D., Glashow, S.L. and Sarid, U., Nucl.Phys.B **309**, 597 (1988)

- [28] E. Zavattini *et al.* [PVLAS Collaboration], arXiv:0706.3419 [hep-ex].  
G. Cantatore, talk given at the 3rd Joint ILIAS-CERN-DESY Axion-WIMPs Training Workshop, University of Patras, Greece (<http://axion-wimp.desy.de>)
- [29] C. Rizzo [BMV Collaboration], 2nd ILIAS- CERN-CAST Axion Academic Training 2006, <http://cast.mppmu.mpg.de/>;  
private communication.
- [30] C. Rizzo [BMV Collaboration], Moriond 2007, <http://moriond.in2p3.fr/J07/trans/thursday/rizzo.pdf>.